Reexamining fission-probability data using $\mathcal{R}$-matrix Monte Carlo simulations: Beyond the surrogate-reaction method

O. Bouland*

CEA, DEN, DER, SPRC, Physics Studies Laboratory, Cadarache, F-13108 Saint-Paul-lez-Durance, France

This article describes an original approach to simultaneously analyzing cross sections and data obtained with surrogate reactions, using an efficient Monte Carlo extended $\mathcal{R}$-matrix theory algorithm based on an unique set of nuclear structure parameters. The alternative analytical path based on the manifold Hauser-Feshbach equation was intensively used in this work to gauge the errors carried by the surrogate-reaction method commonly taken to infer neutron-induced cross sections from observed decay probabilities. The present paper emphasizes in particular a dedicated way to treat ingoing direct reaction and outgoing channels widths correlations and to recall the common absence of class-II states width fluctuation factor in standard codes for calculating average fission cross sections. The present approach opens interesting perspectives on the matter of neutron cross section inference as simultaneously measured fission and γ-emission probabilities become widely available.

I. INTRODUCTION

A wealth of experimental neutron-induced fission cross-section data for actinides and transuranic nuclides has been collected over decades and is still being added. However, the idea to supplement this database with particle-transfer-induced reactions has been raised [1]. This was promoted as long ago as the mid-1960s by Britt *et al.* [2] at Los Alamos Scientific Laboratory. The original goal was to identify the positions of major low-lying collective bands near fission saddle by measuring fission-fragment angular correlations. Within the next decade, Back *et al.* [3] investigated direct nuclear reactions for studying sub-threshold-fission-barrier vibrational structures with relatively low fission probabilities. Over the years, a variety of direct reactions have been used as stripping (d, p) and pickup (p, d) reactions; $(^3\text{He}, p)$, $(^3\text{He}, d)$, and $(^3\text{He}, t)$ charge-exchange reactions; and even two-neutron transfer reactions as (t, p) and (p, t) reactions. The measured fission probabilities were analyzed assuming several simplifications contained in the so-called surrogate-reaction method (SRM). Early promising neutron-induced fission cross-section comparisons [1] made between SRM reduced data and neutron spectroscopy (NS) data led to agreement within 10% to 20% at neutron energy above 2 MeV but exhibited larger deviations below. Major limitations in the application of the SRM were promptly noticed [1,4] with the difficulty to estimate (a) the compound nucleus formation cross section by neutron absorption, (b) the possible influence of the differences between the angular momentum distributions populated by neutron capture and direct reactions, and (c) the validity of the Weisskopf-Ewing (WE) hypothesis on reaction decay probability spin-parity independence [5].

During the past decade, surrogate reactions received renewed interest in terms of simulation [6,7] and experimental investigation (on the spur of study [8]; see also a list of measurements in Ref. [9]). From the very beginning [1], the SRM has been thought to be very helpful when infering cross sections for target material with unsuitable lifetimes (less than several days) or with high radio toxicity. The present design of advanced reactor systems (e.g., accelerator-driven systems and generation IV nuclear power reactors) strengthens the need for conclusive determination of the confidence that can be put in surrogate data feedback. Two clear benefits are expected: better nuclear data assessment for standard reactor fuel nuclides and actual experimental alternatives to achieve suitably evaluated "neutron-induced" cross-section data for more exotic nuclei, as already introduced by Britt and Wilhelmy [4] in the 1970s.

Using energy derivative of probabilities, the authors of the study [10] have recommended not using the WE approximation to extract neutron-induced capture or fission cross sections from surrogate-reaction data. Instead, the authors suggested using these derivatives to extract complementary information to NS such as fission barrier heights. Carrying approximations was understandable in the 1970s because of computer limitations, lack of precise information on nuclear level densities across the deformation, and difficulties in achieving confident optical model calculations over a large range of nuclides. Nowadays, the bulk of those approximations can be overridden even if difficulties persist in the estimation of the various direct, pre-equilibrium, and compound nucleus components of the reaction cross section.

In a previous paper [11], we have discussed the actual possibility of carrying one-dimensional fission barrier extended R-matrix calculations accurate enough to make predictions of low-energy neutron-induced fission cross sections according to the isotopes of a given isotopic chain for which no NS measurements exist.

---

*olivier.bouland@cea.fr

However, in that study, reasonable predictions were made also possible because of the use of fission probabilities induced by surrogate reactions.

This "surrogate-reaction data" aspect was not documented in the earlier publication and is the first aim of the present article. Present analyses cover the 4- to 8-MeV excitation energy range, meaning the domain below and above neutron emission threshold (S_n) that is the most impacted by the SRM hypotheses. One imagines that below S_n, where only γ- and fission decays compete, there are few arguments to expect better agreement between NS and surrogate data in a matter of fission than in terms of capture cross section. Ultimately, I would like to demonstrate that representation of transfer-induced decay probabilities can indeed bring valuable complementary information in terms of cross-section evaluation for nuclear reactor applications.

This article is organized as follows. An overview of surrogate-reaction studies and the associated modeling strategy is first discussed. This is continued with the description of our original approach for surrogate-reaction data that was made available using the in-house AVXSF-LNG (AVerage CROSS Section Fission–Lynn and Next Generation) program. This makes possible the investigation of the behavior of the manifold Hauser-Feshbach equation components whenever surrogate reactions are involved, namely spin-parity population fractions, in-out channel width fluctuation correction factors, and reaction decay probabilities based in this work on the efficient Monte Carlo extended $\mathcal{R}$-matrix theory algorithm. Inaccuracies brought by the SRM in regards to the above baseline in the cases of both fertile and fissile heavy target nuclides are emphasized and pictured across some isotopes of the Pu family. The last section reviews the actual potential of the present neutron cross-section inference from surrogate-reaction data and introduces the next stage of our study.

II. SURROGATE REACTIONS AS SUBSTITUTE FOR NEUTRON SPECTROSCOPY

As mentioned in the introduction, surrogate-reaction measurements are a substitute technique to determine reaction cross sections for nuclei that are difficult to measure directly by NS or to predict with some degree of confidence from systematics or theory. The surrogate technique is an alternative to form the nucleus of interest, A^{*},[1] usually formed through NS as $n + (A\text{-}1) \rightarrow A^{*}$, whose decay properties one wants to measure. Alternatively, another projectile-target combination, more accessible experimentally, can be chosen such that projectile + (surrogate target) $\rightarrow A^{*}$ + ejectile. By measuring the number of coincidences between the observable characterizing the exit channel (c') pursued and the ejectile that signals the nucleus to be analyzed, normalized to the total number[2] of surrogate events recorded, the experimental probability $\mathcal{P}_{\mathrm{surr},c'}^{A^{*}}(E_x)$ is derived.

---

[1]To prevent confusion between the NS target nucleus and the compound system, the $\star$ notation is used in this article for the latter such that A (of the element)*.

[2]Actually corrected for the experimental detector efficiency.

A. Historical surrogate modeling

The starting point and appropriate formalism for describing compound nucleus (CN) reactions is Hauser-Feshbach (HF) statistical theory [12], meaning the pure Hauser-Feshbach equation [11] that carries the Niels Bohr approximation of independence between formation and decay processes of a given CN [13]. A more realistic picture of the interaction involves the term $W_{c,c'}$, the customary in- and outgoing channel width fluctuation correction factor (often abbreviated by WFCF). The average partial cross-section $\sigma_{cc'}$ formulation for an entrance channel c and exit channel c' applied to neutron-induced reactions at given neutron energy E_n, using *L-j coupling*; also described as "channel spin formalism" [14, p. 311], is then

$$\sigma_{n,c'}(E_n) = \sum_{J^{\pi}}\Bigg[\sigma_n^{\mathrm{CN}}(E_n, J, \pi)$$
$$\times \sum_{s'=|I'-i'|}^{I'+i'}\sum_{l'=|J-s'|}^{J+s'}\frac{T_{c'}^{J^{\pi(l's')}}(E_{c'})}{\sum_{c''}T_{c''}^{J^{\pi(l''s'')}}(E_{c''})}W_{n,c'}^{J^{\pi}}\Bigg], \quad (1)$$

where $\sigma_n^{\mathrm{CN}}(E_n, J, \pi)$ is the neutron-induced partial compound nucleus formation cross section related to a given (J, π) couple; the expression of which is

$$\sigma_n^{\mathrm{CN}}(E_n, J, \pi) = \pi \lambdabar^2 g_J \sum_{s=|I-\frac{1}{2}|}^{I+\frac{1}{2}}\sum_{l=|J-s|}^{J+s}T_n^{J^{\pi(ls)}}(E_n), \quad (2)$$

with g_J being the statistical spin factor or weight according to total angular momentum J as $g_J = (2J + 1)/[2(2I + 1)]$ and $T_n^{J^{\pi(ls)}}$ being the neutron entrance transmission coefficients.

The SRM postulates that the WFCF can be neglected (equivalent to say $W_{n,c'} \approx 1$) although one knows that this correction is substantial [15] for the limited number of reaction channels observed below 1 MeV above neutron emission threshold energy (S_n), as far as actinide neutron cross sections are concerned. Specialized to fission decay, the amount of correction depends on both the number of Bohr fission channels [16] involved and the magnitude of their average widths [17]. Larger the sub-barrier effect is (in the case of fertile heavy isotopes), larger is the amount of fluctuations: $W_{n,f} \approx 35\%$ at 1 keV neutron-incident energy for fertile isotopes to be juxtaposed with the 20% observed for fissile isotopes. Obviously $W_{n,f}$ tends to unity as the number of opened fission channels increases. In the present study, fluctuation calculations have been carried up to a maximum excitation energy of 2.1 MeV above the neutron binding energy. The question of the actual WFCF behavior above and below neutron emission threshold for both the fission and capture channels in the case of surrogate reactions is among the items inspected in the present article.

The absence of WFCF is indeed the basic hypothesis behind the SRM. Equation (1) switches back to the pure Hauser-Feshbach formulation that can be written in a concise manner as

$$\sigma_{n,c'}(E_n) = \sum_{J^{\pi}}\big[\sigma_n^{\mathrm{CN}}(E_n, J, \pi)\mathcal{B}_{c'}^{J^{\pi}}(E_{c'})\big], \quad (3)$$

where $\mathcal{B}_{c'}^{J^\pi}(E_{c'})$, the CN partial decay probability into channel c', is also commonly referred as branching ratio (BR) to channel c' in the literature related to surrogate reactions. Equation (3) can be factorized as

$$\sigma_{n,c'}(E_n) = \sigma_n^{\mathrm{CN}}(E_n) \sum_{J^\pi} \left[\frac{\sigma_n^{\mathrm{CN}}(E_n, J, \pi)}{\sigma_n^{\mathrm{CN}}(E_n)} \mathcal{B}_{c'}^{J^\pi}(E_{c'}) \right], \quad (4)$$

to make provision for $[\sigma_n^{\mathrm{CN}}(E_n, J, \pi)/\sigma_n^{\mathrm{CN}}(E_n)]$, the fraction of CN formed in a (J, π) state, which is often referred as $\mathcal{F}_n^{\mathrm{CN}}(E_n, J, \pi)$ in the literature. By analogy, one states that

$$\mathcal{P}_{\mathrm{surr},c'}^{A^*}(E_x) = \sum_{J^\pi} \left[\mathcal{F}_{\mathrm{surr}}^{A^*}(E_x, J, \pi) \mathcal{B}_{c'}^{J^\pi}(E_{c'}) \right]. \quad (5)$$

A straightforward connection between neutron-induced cross section and the surrogate probability is routinely made and defines the SR method. Weisskopf and Ewing [5] suggested that BRs could be independent of spin and parity considerations, meaning substituting $\mathcal{B}_{c'}^{J^\pi}$ by $\mathcal{B}_{c'}$. In that case, branching ratios are pulled out of the spin-parity sum in both Eqs. (3) and (5). The combination of the resulting simplified equations leads to

$$\sigma_{n,c'}^{\mathrm{SRM}}(E_n) \equiv \left[\sum_{J^\pi} \sigma_n^{\mathrm{CN}}(E_n, J, \pi) \right] \mathcal{P}_{\mathrm{surr},c'}^{A^*}(E_{c'}), \quad (6)$$

$$\text{since } \sum_{J^\pi} \mathcal{F}_{\mathrm{surr}}^{A^*}(E_x, J, \pi) = \mathbb{1}. \quad (7)$$

At first sight, this *surrogate strategy* supplies a suitable estimate of the intended neutron-induced cross section without any need [Eq. (5)] to be able to (1) measure individual decay probabilities and (2) predict the $\mathcal{F}_{\mathrm{surr}}^{A^*}(E_x, J, \pi)$ excited state population fractions. By using Eq. (6), assumption is made that the CN neutron-induced formation cross section, $\sum_{J^\pi} \sigma_n^{\mathrm{CN}}(E_n, J, \pi)$, can be ideally modeled using suitable optical model potential.

One realizes promptly the following:

(1) The absence of WFCF at least hides issues related to undeniable partial outgoing channel width correlations over the energy range where fluctuations are observed in the data. On the other hand, using the classical definition of WFCF can distort surrogate data to neutron cross-section conversion since one expects conceptual WFCF differences between surrogate and NS measurements.

(2) The straightforward use of the unitarity property [Eq. (7)] washes out (J, π) population fraction disparities expected between neutron-induced and surrogate reactions. On the other hand, stating that final results are not sensitive to the spin-parity decay probability distribution (WE assumption) leads to the same approximated equation (SRM). This goes against insights showing that transfer reactions populate excited state spins that can be twice as high on average as those produced by neutron-induced reactions [18] and that γ and fission BR can be influenced by the angular momentum and parity of the decaying nucleus as discussed in Ref. [9].

The above arguments suggest that successful use of the surrogate reaction method [Eq. (6)] could rely more on a case-to-case situation than on a systematic rule although one expects to fulfill the conditions at higher excitation energy (reaching the so-called WE limit). This is also what I want to clarify across this step-by-step study.

B. Questionable SRM neutron cross-section predictions as a matter of fact

The lack of high confidence level on the use of the historical surrogate conversion technique unfortunately counteracts the convenience of the method. Finally, it would be very fortunate that the SRM will lead to the level of confidence commonly aimed at major actinide neutron-induced cross section evaluations (a few % uncertainty). Surrogate experiments are undoubtedly of great help in the case of poorly known nuclides whose half-lives range from minutes to hours. This is well exemplified by the case of the $(^{243}\mathrm{Pu} + n)$ system for which capture and fission cross-section uncertainties integrated over a high neutron flux reactor spectrum with a significant thermal contribution were respectively estimated as 275% and 118% using the EAF2007/UN data library [19]. Lowering huge uncertainties is clearly doable by complementing the cross-section evaluation process with surrogate data. Beyond that statement, transfer reaction data analysis of fissile target isotope supplies invaluable estimates of barrier heights that lie below neutron separation energy. Figure 16 of Ref. [11], which plots the fission cross section of the $(^{243}\mathrm{Pu} + n)$ system, well testifies to the extreme impact of substantial change in $^{244}\mathrm{Pu}^*$ barrier heights by bringing the nucleus from the fertile to the fissile family. The present $\mathcal{R}$-matrix Monte Carlo simulation does not carry most of the approximations involved routinely by the surrogate strategy or the simplifications adopted in the calculation of the two-peaked fission barrier resonant penetration by Younes and Britt [6,7]. I expect therefore that present step-by-step surrogate demarche will bring convincing arguments in favor of indisputable inclusion of surrogate data in standard evaluation task for a step further toward low-uncertainty-evaluated neutron-induced reaction cross sections. The present work intends to clarify most of the dilemmas raised by recent surrogate analyses [10,20] that suggest one could work with confidence from experimental fission probabilities but not from γ-decay probabilities.

III. DEDICATED LNG APPROACH TO SURROGATE REACTION DATA ANALYSES

From above theoretical background, the fission probability induced by a surrogate reaction can be written as

$$\mathcal{P}_{\mathrm{surr},f}^{A^*}(E_x) = \sum_{J^\pi} \mathcal{F}_{\mathrm{surr}}^{A^*}(E_x, J, \pi) \mathcal{B}_f^{J^\pi}(E_x) W_{\mathrm{surr},f}^{J^\pi}, \quad (8)$$

where $W_{\mathrm{surr},f}$ is the surrogate-dedicated WFCF factor (SWFCF) that corrects for partial channel width fluctuation correlations across flux conservation [15] according to a surrogate reaction. For better display, the excitation energy (E_x) dependence of the SWFCF has been dropped from Eq. (8); I will embrace this notation throughout this paper. I must

stress that the amount of correlation between formation and decay processes is related to the nature of the reaction mechanisms leading to the excited nucleus. The question of the memory preservation plays a major role in surrogate-reaction experiments because of the necessary high energy of the incident charged particle to overcome the Coulomb barrier (with 24 MeV ^{3}He beam in a recent ^{238}U(^{3}He, ^{4}He)^{237}U* measurement [20]); the interaction time being not long enough to wash out any prior history making of fragile support the use of the CN hypothesis.

The accurate simulation of experimental fission probabilities requires the best knowledge of the three quantities involved in the right-hand side of Eq. (8). The description of the LNG approach to deal with those quantities is the aim of this chapter.

A. Excited nucleus spin-parity population as a function of the entrance channel pattern

By reference to Eq. (8), I begin this discussion by focusing on the first ingredient, $\mathcal{F}_{\text{surr}}^{A^*}(E_x, J, \pi)$, whose level of knowledge remains unsatisfactory in terms of surrogate entrance channel pattern. For neutron-induced reactions, the CN formation cross section is satisfactorily derived from appropriate optical-model potential calculations or using the LNG approach [Eq. (2)]. As described in a previous paper [11], the latter involves computing the elastic neutron channel transmission coefficients using the general form established by Moldauer [21],

$$T_n^{J^{\pi(ls)}} = 1 - \exp\left(-2\pi S_l\right), \qquad (9)$$

where S_l is the energy-dependent neutron strength function for given relative orbital momentum l. Literature on heavy nuclides supplies accurate values of S_l only for s- and p-wave elastic channels extracted from resolved resonance region analyses and average cross section fits below 300 keV. For the present demonstration according to the Pu isotopes family, I have simply assumed $S_l = 1.044 \times 10^{-4}$ for even-l waves and $S_l = 1.48 \times 10^{-4}$ for odd-l waves, referring to the empirical rule that implies similar strength function values for even l-waves (respectively for odd l-waves). The even and odd values assumed in this work are mostly within the uncertainties addressed in associated literature ($\pm 0.1 \times 10^{-4}$ and $\pm 0.4 \times 10^{-4}$ at best respectively for s and p waves). One observes that the definition of $\mathcal{F}_n^{\text{CN}}(E_n, J, \pi)$ is analog to put both energy and level parity dependence of the neutron entrance transmission coefficients in the statistical spin factor [Eq. (2)] such that $g_J \rightarrow g_{J,\pi}(E_n)$. For benchmarking the LNG entrance route based on the neutron transmission coefficients by Moldauer against the results obtained more directly from an appropriate optical model potential (as mentioned by Escher *et al.* [9]), I plot in Fig. 1 the distributions of total angular momenta corresponding to the neutron-induced reaction ($n + {}^{235}$U) calculated with the LNG code for selected neutron energies. The foreground plot, corresponding to neutron incident energies $\geqslant 100$ keV, is quite close to Fig. 20 of Ref. [9]. As expected, one observes that J^π excited states other than 3^- and 4^- (s waves) are populated only significantly at high neutron energies.
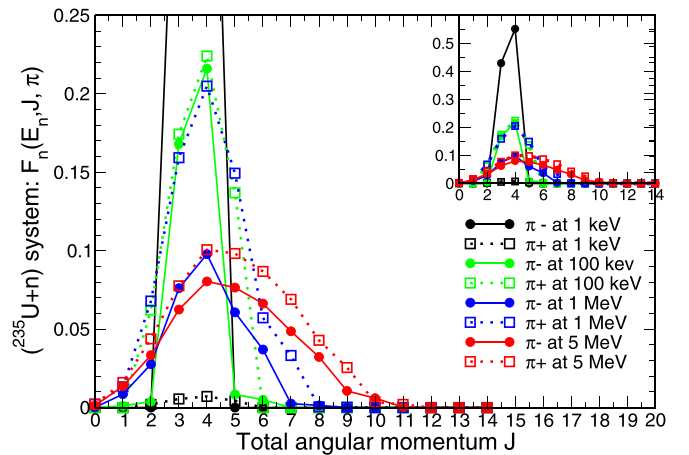

FIG. 1. Distributions of total angular momenta associated to the neutron-induced reaction ($n + {}^{235}$U) resulting from LNG calculations for selected neutron energies. The foreground plot focuses on fast neutron incident energies whereas the inset graphic shows the full picture with an increased vertical scale. Solid lines, connecting dots and addressing negative π (respectively dashed lines with open squares for positive π), are drawn to guide the eye.

In the past decade, literature has pointed out that a condition for the validity of the SRM relies on an idealized matching between neutron-induced and surrogate spin-parity entrance distributions, reading $\mathcal{F}_{\text{surr}}^{A^*}(E_x, J, \pi) \equiv \mathcal{F}_n^{\text{CN}}(E_n, J, \pi)$. Indeed, this equivalence has been questioned since the pioneer times [1]. The answer was inferred from the early finite range interaction distorted-wave Born approximation (DWBA) cross-section calculations for the (t, p), (d, p), and $(^3$He, $d)$ reactions as reported by Back *et al.* (cf. Fig. 7 of Ref. [3]), although those calculations were carrying large uncertainties and would have to be refined. Regarding present paper, I have chosen simply to stick with early direct calculations made by Andersen *et al.* [22] for the particular case of the ^{239}Pu(d, pf) one-particle stripping reaction and with results quoted by Back *et al.* [3] for the remaining (d, p), $(^3$He, $d)$, and (t, p) surrogate reactions. I have used for calculating Eq. (8) the J^π entrance fractions as a function of excitation energy supplied by Andersen *et al.* [22] in graphic form[3] and related to excited states in ^{240}Pu*. In contrast, Ref. [3] returns preferentially the distribution of orbital angular momentum according to the transfer of a particle (separated out of the light incident projectile) to given single-particle shell of the target nucleus. The conversion of the latter to spin-parity distribution has been made in this work following the j-j spin-orbit vectorial coupling scheme. In case of (t, p) reactions on even-even target isotopes carrying zero intrinsic spin and positive parity, the weighting factors, $\mathcal{F}_{\text{surr}}^{A^*}(E_x, J, \pi)$, were obtained from stripping theory where one assumes that the released proton is scattered from the short-range part of the proton-target nucleus interaction as if the dineutron (constituting with the proton the incident triton) was not present.

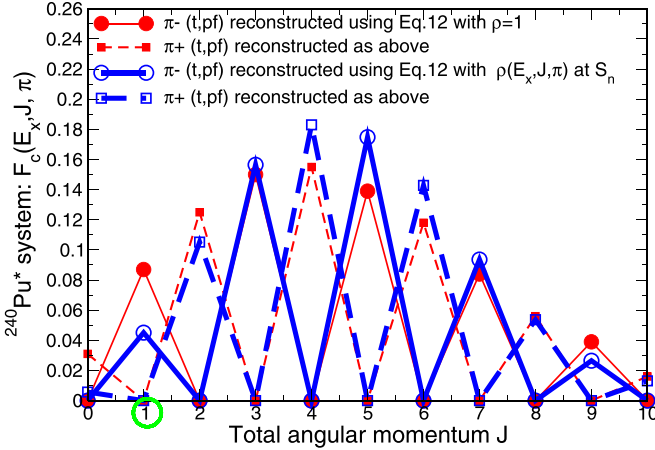[3]With the distance between neighboring curves representing the spin-parity probability of the upper curve.

FIG. 2. The peculiar pattern of the total angular momentum population distribution for the ^{238}Pu$^*(t,p)$ reaction. The above data are retrieved using Eq. (12). Lines connecting dots for negative π (respectively dashed lines with squares for positive π) are drawn to guide the eye. The thin red lines correspond to using Eq. (12) unweighted ($\rho = 1$) whereas the thick blue ones have been obtained with energy-dependent level density, $\rho(E_x, J, \pi)$, as supplied by the approach of Ref. [11]. The green open circle emphasizes the absence of 1^+ states in (t, p) direct reactions.

On this assumption, one can consider a two-body problem with a dineutron trapped into a shell with single-particle-type character of the target nucleus. The excited nucleus total spin is set up from the coupling of the spin of the bound residual nucleus (meaning the target nucleus; indexed 0) with the spin of the dineutron cluster (indexed 12). Applying the j-j coupling scheme to this system leads to

$$\overrightarrow{J}_{A^*} = \overrightarrow{I}_0 + (\overrightarrow{i}_{12} + \overrightarrow{l}_{12}), \qquad (10)$$

with $\overrightarrow{i}_{12}$ being the intrinsic spin of the dineutron cluster and l_{12} being the relative orbital angular momentum between the dineutron and the target nucleus. The excited state parity, π_{A^*}, is ruled accordingly

$$\pi_{A^*} = (-1)^{l_{12}} * \pi_0 * \pi_{12}, \qquad (11)$$

with π_{12} and π_0 being the respective parities of the dineutron cluster and even-even target nucleus (meaning $\pi_0 = 0^+$). If one assumes also antisymmetrical intrinsic spin character ($i_{12} = 0$) and positive parity for the dineutron cluster, the exact equivalence $J_{A^*} \equiv l_{12}$ is verified. Since the parity of the excited state is also driven by the even or odd character of l_{12}, even J are built solely with positive parity and odd J with negative parity. In the case of symmetrical intrinsic spin ($i_{12} = 1$), the conversion will lead to additional possibilities as $| l_{12} - 1 | \leqslant J_{A^*} \leqslant (l_{12} + 1)$ but the lowest single-particle state, $^3P_0$ in spectroscopic notation, is expected to occupy a higher shell and is thus less favored. Figure 2 illustrates that peculiar pattern for triton-induced direct reactions on even-even (0^+) target nucleus where only *natural-parity*[4] states

---

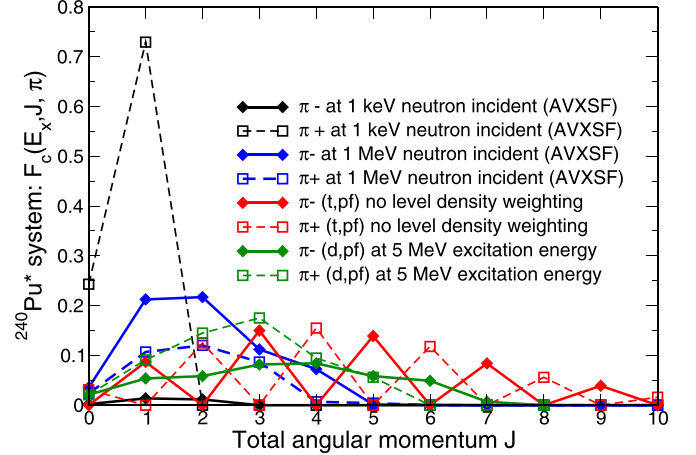[4]Meaning positive-parity states of even angular momenta and negative-parity states of odd angular momenta.

FIG. 3. Calculated population distributions of total angular momentum for the ^{240}Pu* formed by a neutron-induced reaction ($n + {}^{239}$Pu) at 1 keV and 1 MeV, by a ^{238}Pu(t, p) reaction (Back *et al.* [3]), and by a ^{239}Pu(d, p) reaction (Andersen *et al.* [22]). Solid lines connecting diamonds and addressing negative π (respectively dashed lines with open squares for positive π) are drawn to guide the eye.

are populated ($i_{12}^\pi = 0^+$). Expanding the context of the (t, p) reactions to non-even-even target nuclei, the spin-parity state population distribution expected under *j-j coupling* is

$$\mathcal{F}_{\text{surr}}^{A^*}(E_x, J, \pi)$$
$$= \rho(E_x, J, \pi) \sum_{j=|J-I|}^{J+I} \sum_{l=|j-i|}^{j+i} \frac{P_l \delta(\pi_J, \pi_i \pi_I (-1)^l)}{\sum_{j=|J-I|}^{J+I} \sum_{j=|j-i|}^{j+i} 1} \qquad (12)$$

with

$$P_l = \frac{(2l+1)\sigma_l}{\sum_l (2l+1)\sigma_l},$$

with $\sigma(l)$, the angular momentum transfer cross section given by Ref. [3] and $\rho(E_x, J, \pi)$, the excited nucleus level density (LD). The final expression for $\mathcal{F}_{\text{surr}}^{A^*}(E_x, J, \pi)$ is normalized, consistent with Eq. (7).

Figure 2 obviously invalidates the hypothesis of comparable neutron and (t, p) reaction spin-parity entrance distributions. Spin-parity distribution comparisons with less quirky signatures as involved in (d, p) processes deliver a similar verdict as exemplified by the ^{239}Pu$(d, p)^{240}$Pu* DWBA distribution calculated by Andersen *et al.* [22] (shown here in Fig. 3). The pattern of the positive-parity population distribution, which is closed to a truncated Gaussian distribution centered about $J = 3\hbar$ with dispersion of $1.5\hbar$, would require high-energy neutron-induced reactions.

B. Modeling of in- and outgoing channel width fluctuation correction factors

One knows from Moldauer [21] that the in- and outgoing channel width fluctuation correction factor, $W_{c,c'}$, plays a major role in low-energy neutron-induced reactions in averaging over partial width distributions to assess average cross sections. This was well quantified in a model comparison by Hilaire *et al.* [15]. In the matter of surrogate reactions, the question of the correlation between entrance and exit channel

widths is obviously sensitive because it depends on the direct entrance reaction type. For instance, in a (t, pf) reaction, considered later in this paper, two neutrons in paired orbits are stripped into the field of a target nucleus that has two neutrons less than the residual nucleus. Its formation cross section is then proportional to the reduced width,[5] $\gamma_{2n'}^2$, for a "dineutron" single-particle channel for which the reaction energy threshold is close to twice the neutron separation energy. I guess that the correlation between the entrance dineutron reduced width and the similar decay channel reduced width of the compound system excited state, restricted over the studied low excitation energy range to (1) single-neutron emission (above S_n), (2) γ emission, and (3) fission will likely be of third order magnitude and can be easily ignored. However, other direct reaction entrance channels that have been considered in this work as (^{3}He, d) and (^{3}He, t) charge-exchange reactions where a proton is pulled into the field of a target nucleus (e.g., ^{240}Pu) must be considered with more attention. The question of the correlation between entrance single-particle proton width and compound system proton decay channel width is, however, simplified by the fact that above the proton emission energy ($S_p = 4.48$ MeV in ^{241}Am), the charged-particle penetrability becomes appreciable only when the exit proton energy approaches the Coulomb barrier value, meaning $B \approx [1.44\,Z_p Z_{240}]/[1.60[A_p^{1/3} + A_{240}^{1/3}]] \approx 11.7$ MeV and thus its proton emission width. In the matter of stripping (d, p) reactions, the question of the correlation between formation and decay widths is more tricky. Later reaction can be illustrated as a deuteron sweeping past the target nucleus with its proton repelled by the Coulomb field and the neutron coming into close enough proximity to the target to be pulled into one of the (bound) single-particle orbit in the nuclear field. If the excitation energy of the single-particle neutron is above neutron emission energy, the corresponding elastic neutron emission width is nonzero and there might be interference between both partial widths. Theory related to width fluctuation effects for that type of surrogate reactions has been developed by Kerman and McVoy [24] but is not handled

in present work because of the following reasons: For fissile isotopes, particle-transfer-induced fission data are studied to infer fission barrier height values lying below the neutron separation energy. In addition, right above S_n, the neutron width remains small compared to the total width; this statement is still reinforced since surrogate reactions populate in general high total angular momentum levels. In consequence, the assumption that the formation width does not participate in the width fluctuation correction sounds quite reasonable also for (d, p) reactions. The present SWFCF calculations have been carried without considering any relationship between formation channel and analogous decay channel such that one can state

$$\left\langle \frac{\mathcal{F}_{\mathrm{surr}}^{A^*} \Gamma_{c'}}{\Gamma_{\mathrm{tot}}} \right\rangle \equiv \mathcal{F}_{\mathrm{surr}}^{A^*} \left\langle \frac{\Gamma_{c'}}{\Gamma_{\mathrm{tot}}} \right\rangle = \mathcal{F}_{\mathrm{surr}}^{A^*} \left\langle \frac{\Gamma_{c'}}{\sum_j \Gamma_j + \Gamma_{\mathrm{cst}}} \right\rangle$$
$$= \mathcal{F}_{\mathrm{surr}}^{A^*} \frac{\langle \Gamma_{c'} \rangle}{\left\langle \sum_j \Gamma_j + \Gamma_{\mathrm{cst}} \right\rangle} W_{\mathrm{surr},c'}, \quad (13)$$

where Γ_{cst} represents a global nonfluctuating lumped channel merging various constant (cst) components, meaning total radiative decay, delayed fission in the second well, and fission over outer barrier continuum transition states. Very small channel width values corresponding to the highest orbital angular momenta are also put in Γ_{cst} in order to speed up the computation of fluctuation factors as well as weakly fluctuating channel contributions, according to a width distribution degrees of freedom (DoF) larger than 2.0 units. The entrance surrogate channel width would be identified as the dissimilar entrance single-particle channel width. $\sum_j \Gamma_j$ regroups the most fluctuating decay channel widths (i.e., largest particle emission and fission channels). Numerical evaluation of SWFCF in the framework of Hauser-Feshbach statistical theory is carried out analogously to the general single variable integral established by Dresner [25], assuming that the partial width of given channel, c, can be represented by a χ^2 distribution with ν_c degrees of freedom. This results in

$$\left\langle \frac{\Gamma_{c'}}{\sum_j \Gamma_j + \Gamma_{\mathrm{cst}}} \right\rangle_{\lambda_I} n = \frac{\nu_{c'}}{2} \prod_j \left(\frac{\nu_j \Gamma_{\mathrm{cst}}}{2 \bar{\Gamma}_j} \right)^{\frac{\nu_j}{2}} \int_0^\infty dt \left[e^{-t} \left(t + \frac{\nu_{c'} \Gamma_{\mathrm{cst}}}{2 \bar{\Gamma}_{c'}} \right)^{-1} \prod_j \left(t + \frac{\nu_j \Gamma_{\mathrm{cst}}}{2 \bar{\Gamma}_j} \right)^{-\frac{\nu_j}{2}} \right], \quad (14)$$

while that quantity expressed for the lumped channels reduces to

$$\left\langle \frac{\Gamma_{\mathrm{cst}}}{\sum_j \Gamma_j + \Gamma_{\mathrm{cst}}} \right\rangle = \prod_j \left(\frac{\nu_j \Gamma_{\mathrm{cst}}}{2 \bar{\Gamma}_j} \right)^{\frac{\nu_j}{2}} \int_0^\infty dt \frac{e^{-t}}{\prod_j \left(t + \frac{\nu_j \Gamma_{\mathrm{cst}}}{2 \bar{\Gamma}_j} \right)^{-\frac{\nu_j}{2}}}. \quad (15)$$

The SWFCF is among the items I want to emphasize in this paper. Beyond its specific shape and magnitude pattern (illustrated later in the text), I recall that statistical

treatment specialized to fission decay probability involves an additional width fluctuation correction factor brought by class-II state properties, the so-called W_{II} [17], whose impact is usually disregarded in standard average cross-section evaluation codes. For the present illustration of $W_{c,c'}$ and W_{II} effects, a modified formulation of the analytical Eq. (8) is envisioned although the real situation avoids decoupling fine structure width fluctuations from class-II state width fluctuations brought by double fission barrier treatment. More reliable calculations based on Monte Carlo simulations are

---

[5]γ_c^2 is known as the reduced width whereas γ_c is the reduced width amplitude which is the value of the internal eigenfunction X_λ at the entrance to channel c. Observed width, Γ_c, and reduced width are connected [23] through centrifugal and Coulomb penetrabilities, meaning $\Gamma_c^{1/2} \equiv \gamma_c \sqrt{2P_c}$.

favored in this work for valuable partial cross sections or surrogate-reaction probabilities modeling.

The usual WFCF quantities needed in this work to calculate NS average partial cross sections were implemented on the grounds of Eqs. (17) and (16) of Ref. [26] that correspond respectively to treatment of the elastic ($c' = c$) and nonelastic partial channels ($c' \neq c$). Because its formulation is analogous to latter nonelastic partial channel width correlation treatment, Eq. (14) sets a weak relationship between the entrance surrogate-reaction channel width and any exit reaction channel.

C. In-house fission decay probability calculation using the Monte Carlo route

A major difficulty in fission decay probability calculations lies in poor model representation of the fission channel. Consistently to common state-of-art evaluation, this study uses the well-known Hill and Wheeler [27] transmission coefficient formula that is based on two common approximations: a unique one-dimensional fission path and a representation of each single-humped fission barrier as inverted parabola. The approximation of a unique one-dimensional fission path appears well justified in the case of the plutonium isotopes I study here, as predicted by the static finite-range droplet model (FRDM) calculations of Möller *et al.* [28]. The asymmetric mode remains the main contribution to fission until past the outer saddle point, from which the symmetric path becomes relevant. Even when these two modes coexist, they remain distinct because of the existence of a significant separating ridge (at least 1 MeV above the upper valley). One can nevertheless argue that triaxiality is observed at the inner barrier (see Table XI of Ref. [29]) and must be taken into account somehow. This is achieved in our calculations by modulating, for instance, the circular frequency associated to the γ-axis primary phonon vibration excitation. Whenever the axial symmetry is recovered (at the outer barrier, for instance), the softness toward this axis is released by putting a high phonon quantum value. Our original approach in the matter of A. Bohr transition states above fundamental fission humps has been described in Ref. [11]. It relies on *ad hoc* sequences of individual transition states above fundamental barriers at low excitation energies built consistently with our combinatorial quasi-particle-vibrational-rotational (QPVR) calculations that are performed to construct LD on top of the individual transition state sequence. Over the upper energy range, detailed resonance structure is of much less importance. The fission cross section mainly depends on both level densities of the compound nucleus at barrier deformations and the level density of target nucleus at normal deformation, which controls the competing inelastic neutron scattering reaction. Therefore, special attention was paid to modeling level density functions and interpreting fits to them where these are required for matching neutron-induced cross-section data. Regarding the validity of the inverted parabola approximation, we have shown in our previous paper [11] (Fig. 7) that this latter assumption clearly appears to be well justified only for the heaviest isotopes of plutonium (above mass 241). I emphasize that the present work is restrained to inverted parabola fission barrier calculations.

I can then argue that present fission decay probability calculations carry the most accurate and physical approach available routinely for low excitation energy (i.e., lower than second-chance fission) fission cross-section calculations. In this sense, this is a smart complement to the work by Younes and Britt [6,7] on the inference of neutron-induced fission cross sections by fission-probability data regarding to the Pu isotope family. In particular, present theory is based on an extension of $\mathcal{R}$-matrix theory to the fission deformation variable as outlined by Bjornholm and Lynn [30]. Since this theory has been exhaustively described in Ref. [11], I will focus here on what is essential to ensure a clear understanding.

1. Typical analytical coupling formulas modeling double-humped fission barrier potential

a. Statistical regime. For excitation energies above the fission barrier, the fission transmission coefficient is calculated using the well-known statistical regime equation, which is derived as follows,

In the framework of a double-humped fission barrier whose two humps are uncorrelated and each described by a (single-humped) Hill-Wheeler form [27], standard probability treatment (Ref. [30], p. 752) returns the probability[6] to fission from an excited state in the first well of the fission barrier as

$$\mathcal{B}_{I \to f} = \frac{T_A T_B}{(T_A + T_I)(T_A + T_B + T_{II}) - T_A^2}, \tag{16}$$

where T_I and T_{II} are the damping coefficients respectively in the first and second wells. T_I and T_{II} include particle emissions and electromagnetic decays. T_A and T_B are the total fission transmission coefficients over inner A and outer B humps, respectively. The above equation can be reformulated as a function of the whole fission barrier transmission coefficient T_f, according to a Hauser-Feshbach-type equation,

$$\mathcal{B}_{I \to f} = \frac{T_f}{T_f + T_I + T_{II}}. \tag{17}$$

Making the equivalence between Eqs. (16) and (17) leads to

$$T_f = \frac{(T_I + T_{II})T_A T_B}{T_A T_{II} + T_I(T_A + T_B + T_{II})}. \tag{18}$$

Equation (18) can be further modified as

$$T_f = \frac{T_A T_B}{T_A + \varepsilon(T_B + T_{II})}$$

$$\text{with } 0 \leqslant \varepsilon \equiv \left(1 - \frac{T_{II}}{T_I + T_{II}}\right) \leqslant 1. \tag{19}$$

Two limiting cases must be mentioned:

(1) No damping in the first well, meaning $T_I = 0$ or equivalently

$$\varepsilon = 0 \to T_f = T_B. \tag{20}$$

---

[6]Probability or branching ratio regarding present surrogate-reaction topic.

(2) No damping in the second well, meaning $T_{II} = 0$ or equivalently

$$\varepsilon = 1 \rightarrow T_f = \frac{T_A T_B}{T_A + T_B}. \tag{21}$$

Equation (21) is the well-known statistical regime formula that is used in the present study at excitation energies above the fission barrier. I emphasize that Eq. (19) corresponds to the most exact equation that covers in particular the two limiting situations above. Configurations favoring Eq. (20) are expected to happen as, for instance, in heavy-ion collision experiments forming high total angular momentum excited states at excitation energies below neutron separation energy. Over the same energy domain as the present study, not just neutron emission is blocked but also γ decays. The fission across the very low fission barrier of the superheavy compound system formed remains as a unique decay mode. Over those atypical configurations, the error brought by classic use of Eq. (21) would have to be examined carefully.

b. Sub-barrier excitation energies. At sub-barrier and near-barrier excitation energies, the detailed structure of class-II levels has significant impact on T_f. Since the bulk of the strength of T_f is concentrated in a narrow energy interval at about a class-II level, the actual average fission probability magnitude will be rather recovered by an average over the large energy intervals separating the class-II states. The consequence is a noticeable reduction of the average fission probability resulting from the use of Eq. (21). This is equivalent to considering the fission transmission coefficient as a sum of the direct term with an indirect term, the latter manifesting the class-II nucleus structure. On the assumption of uniform class-I and class-II level spacings (so-called picket fence model), Lynn and Back [31] have worked out a formulation for the average fission probability $\mathcal{B}_f$, now incorporating the intermediate structure (indexed *IS*) that, in the limit of complete damping in the second well (i.e., no direct fission, only indirect fission after inner barrier tunneling) reduces to

$$\mathcal{B}_{f,IS} = \left[1 + \left(\frac{T_I}{T_f} \right)^2 + \left(\frac{2T_I}{T_f} \right) \coth\left(\frac{T_A + T_B}{2} \right) \right]^{-1/2}. \tag{22}$$

I emphasize that a variety of analytical formulas valid only under specific class-I/II coupling situations are quoted in literature [30]. Whenever the fission model contains the class-II states nucleus structure, a correlation factor between the class-II states (λ_{II}) coupling, $\Gamma_{\lambda_{II(\downarrow)}}$, and fission, $\Gamma_{\lambda_{II(\uparrow)}}$, widths is expected. Using again the general form established by Moldauer [21], one can define $T_A = 2\pi \langle \Gamma_{\lambda_{II(\downarrow)}} \rangle_{II} / D_{II}$ and $T_B = 2\pi \langle \Gamma_{\lambda_{II(\uparrow)}} \rangle_{II} / D_{II}$ with $\Gamma_{\lambda_{II,tot}} \approx \Gamma_{\lambda_{II(\downarrow)}} + \Gamma_{\lambda_{II(\uparrow)}}$ and D_{II}, the corresponding total width and mean resonance spacing of the class-II states:

$$\left\langle \frac{\Gamma_{\lambda_{II}\downarrow} \Gamma_{\lambda_{II}\uparrow}(\mu)}{\Gamma_{\lambda_{II}}} \right\rangle_{\lambda_{II}} = W_{II}(\mu) \frac{\langle \Gamma_{\lambda_{II}\downarrow} \rangle \langle \Gamma_{\lambda_{II}\uparrow}(\mu) \rangle}{\langle \Gamma_{\lambda_{II}} \rangle}. \tag{23}$$

In view of Eq. (23), Eq. (1) becomes for a fission reaction

$$\sigma_{nf}(E_n) = \sum_{J^\pi} \left[\sigma_n^{\mathrm{CN}}(E_n, J, \pi) \right.$$
$$\left. \times \left[\sum_{\mu \in J^\pi} \mathcal{B}_f(E_f, \mu) W_{II}(\mu) \right] W_{n,f}^{J^\pi} \right], \tag{24}$$

or analogously in terms of surrogate-reaction decay probability

$$\mathcal{P}_{\mathrm{surr},f}^{A^*}(E_x) = \sum_{J^\pi} \left\{ \mathcal{F}_{\mathrm{surr}}^{A^*}(E_x, J, \pi) \right.$$
$$\left. \times \left[\sum_{\mu \in J^\pi} \mathcal{B}_f(E_x, \mu) W_{II}(\mu) \right] W_{\mathrm{surr},f}^{J^\pi} \right\}. \tag{25}$$

Recent calculations [17] have reported the global amount of correction brought by W_{II} [Eq. (23)] that is of the same order of magnitude for fertile (20%) and fissile (10%) target nuclides, although the sub-barrier effect, as expected, is much smaller in the fissile case. This returns a 10% to 20% estimate on the error brought by the absence of W_{II} (mainly) below 300-keV incident neutron energy in calculated average fission cross section by codes that rely only on the standard width fluctuation corrected Hauser-Feshbach formulation [Eq. (1)].

However, still more trouble is expected because of the IS pattern in average cross-section calculation. Classically, one assumes that statistical fluctuations of the class-II partial fission widths, $\Gamma_{\lambda_{II}\uparrow}$, exhibit an independent Porter-Thomas [32] ($\nu = 1$) distribution across n fully open Bohr fission channels. If each average partial fission width according to a given outer Bohr channel is equal, then the distribution of the total fission widths is ruled by a χ^2 law with $\nu_f = n$ DoF. In Hauser-Feshbach statistical theory with adequate $W_{n,f}$ factor, the associated DoF ν_f must be equal to the number of open channels at the outer barrier. However, the IS, which lowers the transmission across the outer fission channels, manifests as an actual reduction of ν_f. In our calculations, each effective value of ν_f has been derived by maximum likelihood method from the value of the double barrier fission width averaged over 1600 Monte Carlo trials. The results were presented [17] as a function of the inner barrier transparency for a range of fully open outer barrier channels. The conclusion was that an ideal one fission channel according to a single-hump situation (i.e., no IS and $\nu_f \rightarrow 1$) is recovered only when the inner barrier DoF, ν_A, is sizable. In any other coupling situation, ν_f is strongly reduced by the IS ($0 < \nu_f < 1$) and any subsequent $W_{n,f}$ calculation will have to be corrected accordingly. In practice, this is equivalent to substituting $W_{n,f}(\nu_f)$ by $W_{n,f}(\nu_f^{\mathrm{eff}})$ in Eq. (24) [respectively for Eq. (25)] with ν_f^{eff}, the effective DoF. This is another source of error that is usually compensated for by another parameter during the fitting process on experimental data.

2. Monte Carlo calculations of the intermediate structure

Real situations avoid the decoupling hypotheses of Eq. (24) since class-I and class-II state width statistical properties are obviously correlated across the intermediate fission barrier. Although Eq. (24) supplies valuable estimate of the average neutron-induced fission cross section, an exact solution for this equation relies on the possible derivation of an analytical expression pertaining to the actual coupling strength situation. A powerful alternative to analytical formulas is our Monte Carlo–type (MC) method [11], which presents the advantage of computing average cross sections and average surrogate-reaction decay probabilities, taking full account of the various parameter statistical fluctuations under the exact coupling conditions. Our MC approach simulates R-matrix resonance properties, relevant to each selected class-II state and neighboring class-I states (over at least a full class-II energy spacing), using a chain of pseudorandom numbers for a fine-tuned selection process based on both level width and spacing statistical distributions with suitable averages. For backup, the obtained MC average total cross section (respectively, the total decay probability) according to given spin parity is compared with the entrance channel total cross section (respectively, the excited nucleus population fraction), making an allowance to slight magnitude renormalization whenever computing accelerations carried by the MC procedure bring differences. This MC procedure carries the compact formulation of the previously cited equations, meaning

$$\sigma_{nf}(E_n) = \sum_{J^\pi} \left[\sigma_n^{CN}(E_n, J, \pi) \mathcal{B}_{f,MC-xs}^{J^\pi}(E_f) \right], \qquad (26)$$

in terms of MC fission cross sections or surrogate reactions MC fission probability,

$$\mathcal{P}_{surr,f}^{A^*}(E_x) = \sum_{J^\pi} \left[\mathcal{F}_{surr}^{A^*}(E_x, J, \pi) \mathcal{B}_{f,MC-surr}^{J^\pi}(E_x) \right] . \quad (27)$$

D. In-house γ decay probability Monte Carlo calculation using LNG

One realizes immediately that calculating Eqs. (26) or (27) involves simultaneous transmission coefficient calculations of competing γ channels, neutron elastic channel(s), as well as open inelastic channels to satisfy to total flux conservation. As mentioned in Sec. III A, neutron channels are modeled on the ground of Eq. (9) but the calculation of γ-channel transmission coefficients borrows the classic narrow resonance approximation limit according to weak strength functions, meaning

$$T_\gamma^{J^\pi} = 2\pi \frac{\langle \Gamma_\gamma^{J^\pi} \rangle}{D_{J^\pi}}, \qquad (28)$$

where D_{J^π} is the mean average resonance spacing for given spin J and parity π. However, the question of the energy dependence below S_n for the fissile isotopes is also sensitive. The LNG default route involves the equiprobable parity composite prescription of Gilbert and Cameron [33] for D_{J^π} and parameters have been adjusted to reproduce the experimental s-wave mean level density at S_n (see Table III [11]). With the present objective of modeling that surrogate data as well as possible,

one cannot afford the default semiempirical approach and I will rather rely on the QPVR LD procedure [11]. For an even-even excited nucleus, the lowest excited states are built solely from pure collective excitations up to the energy of the breaking of a neutron or proton pair, whereas the spectrum of odd-N, even-Z fissioning nuclei involves single-quasineutron states that carry vibrational states. As excitation energy increases, meaning above the breaking of a neutron or proton pairing energy for an even-even nucleus, multi-quasiparticle states carrying multiphonon vibrational states show up in the level spectrum. Finally, rotational bands following classical rules are built on those bandheads. QPVR LD have also been used for better estimates of $\langle \Gamma_\gamma^{J^\pi} \rangle$. Full model description and numerical applications are available in Refs. [11,34].

IV. SCANNING THE SURROGATE-REACTION METHOD

A. WFCF versus SWFCF shape and magnitude

Following equations formulated above, I am able to quantify the global impact of $W_{n,f}$, $W_{surr,f}$, and W_{II} for both categories of heavy nuclides: Those which are fertile or fissile according neutron-induced reactions. Reader might also refer to the exhaustive study by Hilaire *et al.* [15] about the various approximated WFCF formulas and expectations when applied to heavy and light nuclides. I start this chapter by verifying if WFCF expected features are reproduced by present numerical calculations.

1. WFCF features according to heavy target nuclides

a. Fertile nuclides. I illustrate this category with ^{241}Pu* formed by neutron capture. One should recover in terms of WFCF the well-known pattern of a medium-mass target nucleus with substantial capture cross section. Below fission threshold, meaning a few hundred of keV according to inner and outer fundamental barrier heights (labeled V_A and V_B), only scattering and capture reactions are opened. In addition, if the neutron energy lies below inelastic threshold ($E_n < 50$ keV on Fig. 4), it all depends on a competition between elastic and capture. Since both cross-section magnitudes are of same order, elastic enhancement is already significant at low energy (larger than +10%; Fig. 5, see $W_{n,n}^{xs}$) but becomes much larger (up to +120%; Fig. 6, see inset) when crossing the inelastic threshold energy. The observed drop in the inelastic cross section is quite large (about −40%) and in agreement with the amount of flux redistributed to the elastic channel. The depreciation of the inelastic cross section is still amplified by the gradual disappearance of the competitive capture channel which is not capable of bringing back some neutron flux to the elastic (in contrast to low energies where the decrease in the capture cross section reaches −25%). The WFCF correction applied on the fission cross section is substantial ($W_{n,f}^{xs} \approx 0.80$) for this fertile target isotope and reaches unity only above 1 MeV, where the total number of open channels involved becomes very large (attested on Fig. 4 by full opening of both fission and inelastic channels). The specific correction due to the statistical fluctuations of the class-II state widths is rather constant ($W_{II}^{xs} < 0.80$) over the whole fluctuation range until the total number of playing
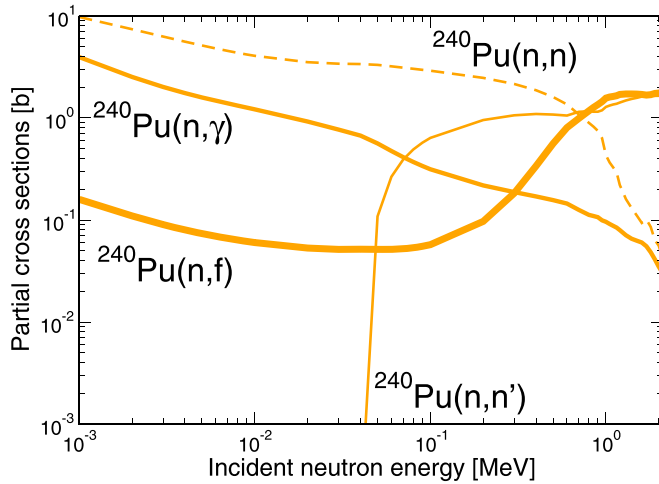
FIG. 4. ^{240}Pu neutron-induced partial cross sections computed analytically with LNG. Thick, medium-thick, and thin solid curves and dashed line correspond respectively to the (n, f), (n, γ), total inelastic (n, n'_{tot}), and elastic (n, n) compound nucleus cross sections.

fission channels becomes large, meaning the energy where the inelastic cross section reaches its plateau and both V_A and V_B – see Fig. 4 – are actually surpassed.

b. Fissile nuclides. Recommending the case of the ^{240}Pu* formed by neutron interaction sounds to be the logical extension to raise the issue of fissile nuclides. Unlike the fertile case, the amount of flux redistributed to the elastic channel is quite large right above S_n (inset of Fig. 8) since low-energy
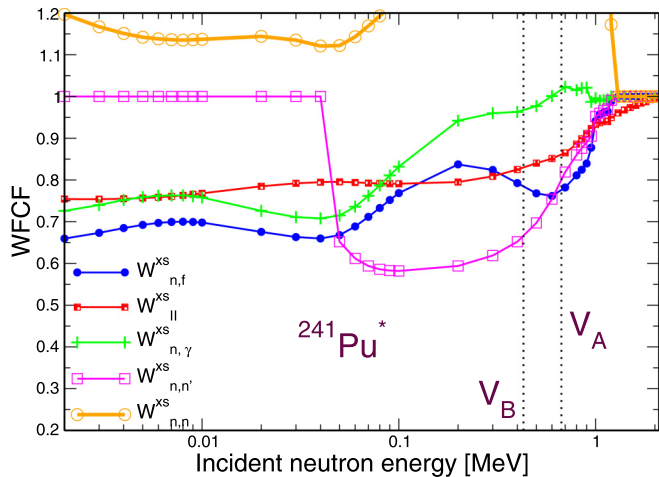
FIG. 5. Comparison of the $W_{n,f}$, W_{II}, $W_{n,\gamma}$, $W_{n,n}$, and $W_{n,n'}$ patterns for the (^{240}Pu $+n$) compound nucleus involved for calculating average cross sections (superscript label *xs*). The WFCF coefficients displayed must be seen as global coefficients related to each partial reaction (elastic, inelastic, fission, and capture) but integrated over all J^π compound nucleus excited states. Note that present $W_{n,f}$ and W_{II} curves differ from Ref. [11] (Fig. 4) by their smoother character because Dresner numerical integrations are here performed on the whole fluctuating energy range. The default route involves Dresner integration and appropriate WFCF asymptotic formulas to save computing time.
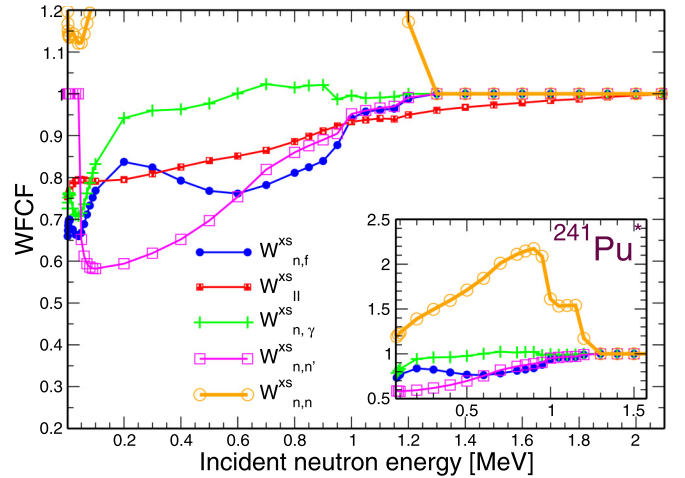
FIG. 6. Same as Fig. 5 but using *x*-axis linear scale. In addition, an inset image displays the whole WFCF pattern, showing the well-known strong elastic enhancement.

fission and capture cross section magnitudes are comparable (Fig. 7). Above first inelastic threshold, and by analogy to the ^{241}Pu* case, the elastic enhancement strength is strongly supported by the flux borrowed from the inelastic channels. The W_{II}^{xs} (Fig. 8) correction cannot be neglected ($\approx 10\%$ up to $S_n + 300$ keV) although the average sub-barrier effect that lowers the *statistical regime* fission probability is much smaller for a fissile than for a fertile heavy nuclide (Fig. 9).

2. Foreseen WFCF features for surrogate reactions

According to the WFCF *extreme limit* that I postulated for surrogate-reaction experiments [Eq. (13)], one can now address the main features as a function of the excited nucleus excitation energy. Since I aim to argue on (global) WFCF features according to both neutron-induced and particle-induced transfer reactions, I have chosen to compute SWFCF factors with the neutron-induced population distributions
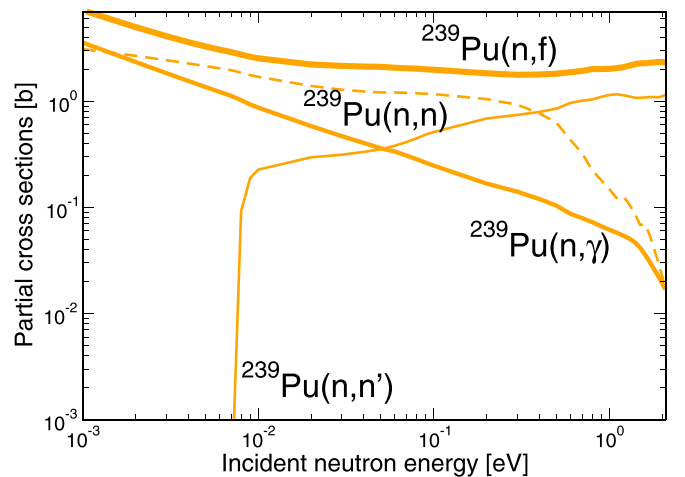

FIG. 7. ^{239}Pu neutron-induced compound nucleus partial cross sections computed analytically with LNG. Legends are identical to Fig. 4.
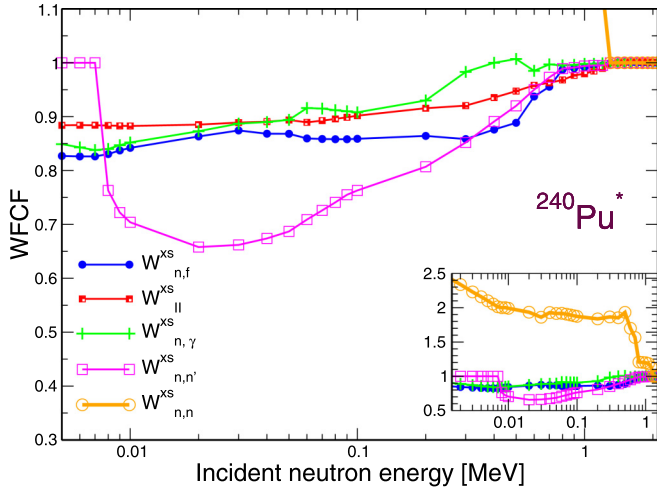
FIG. 8. Comparison of the $W_{n,f}$, W_{II}, $W_{n,\gamma}$, $W_{n,n}$, and $W_{n,n'}$ factors involved for calculating average cross sections (superscript label "xs") according to the (^{239}Pu $+n$) reaction. The inset image displays the whole WFCF picture and shows the well-known strong elastic enhancement.
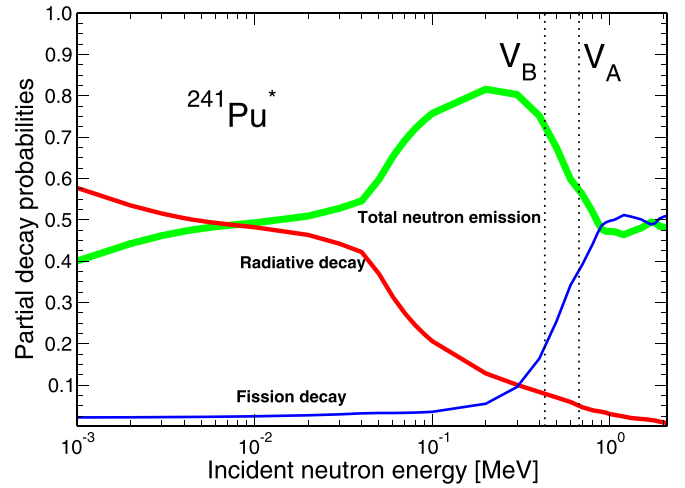

FIG. 10. ^{241}Pu* neutron-fed transfer partial decay probabilities computed analytically with LNG. Thick, medium-thick, and thin solid curves correspond respectively to total neutron emission, radiative, and fission decays.

[i.e., $\mathcal{F}_{\text{surr}}^{A^*}(E_x, J, \pi) \equiv \mathcal{F}_n^{A^*}(E_n, J, \pi)$]. This guarantees a consistent ground for the comparisons. To better understand in terms of SWFCF, one must remember that I postulated no in- and outgoing channel widths correlation but the channel widths correlations between the many exit channels remain preserved.

a. Fertile nuclides. I am now back to the ^{241}Pu* case, but with specialization to "neutron-induced" transfer reactions (called "neutron-fed" in next sections). I will reinforce present argumentation by showing the ^{241}Pu* neutron-fed transfer reaction decay probabilities are defined by Eq. (25). According to the fertile nuclide category, one visualizes in Fig. 10 a very low magnitude for the surrogate-reaction fission decay

probability until fission threshold is surpassed. Right below 1 MeV neutron energy, the radiative decay probability becomes negligible, whereas both the total neutron emission and fission contribute each to half of total decay. In terms of SWFCF, one recovers in Fig. 11 the customary high-energy pattern since each SWFCF tends to unity when the total number of channels involved becomes very large, in practice, above ($S_n + 1.8$) MeV. The absence of elastic channels prevents any classic elastic enhancement and one observes that both radiative and fission decays now endorse the role of the enhanced channels with maximum impact on the γ decay channel, up to +110% of enhancement at ($S_n + 200$) keV. By reciprocity, neutron emission channels are depreciated accordingly to the total amount of reaction rate redistributed. One notices the new role of the neutron emission with residual
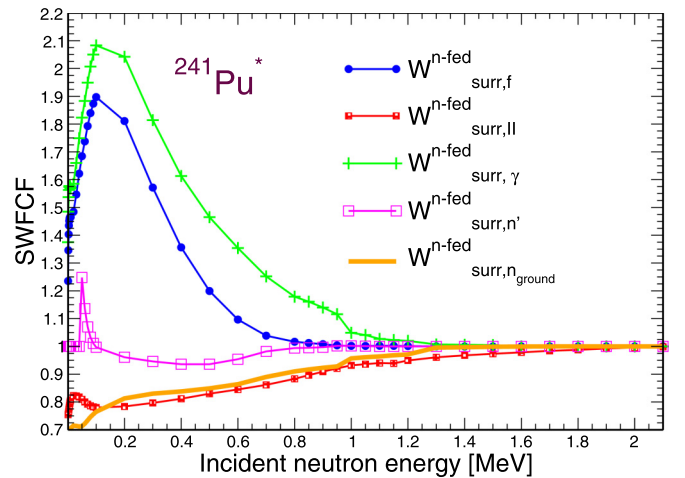

FIG. 9. Sub-barrier tunneling estimates based on the Lynn and Back [31] formulation of $\mathcal{B}_{f,IS}$ [Eq. (22)]. Right above S_n, the maximum of sub-barrier effect recorded for the fissile target nucleus (green solid curve) of about 15% is in contrast to the 80% strong impact according to the fertile case (red dashed curve).

FIG. 11. Comparison of the $W_{\text{surr},f}$, $W_{\text{surr},II}$, $W_{\text{surr},\gamma}$, $W_{\text{surr},n_{\text{ground}}}$, and $W_{\text{surr},n'}$ SWFCF patterns obtained for the ^{241}Pu*. For better comparison, they are calculated with the neutron-incident excited state population [($n - fed$) superscript].
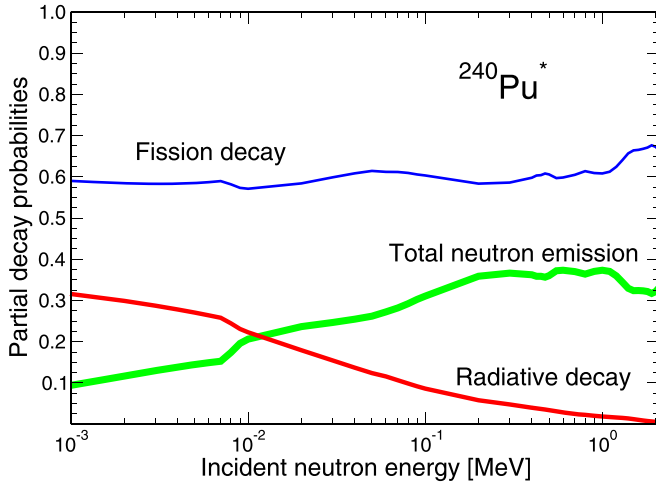
FIG. 12. ^{240}Pu* neutron-induced transfer partial decay probabilities computed analytically over neutron spectroscopy fluctuating energy range. Thick, medium-thick and thin solid curves correspond respectively to total neutron emission, γ and fission decay probabilities.

nucleus in the ground state since this channel represents the largest SWFCF flux contributor ($W_{\text{surr},n_{\text{ground}}}$ curve on Fig. 11) to the capture and fission channels.

b. Fissile nuclides. I refer logically to the ^{240}Pu* case for straightforward comparison with above neutron-incident cross-section WFCF pattern. Once more, I support this argumentation with corresponding computed neutron-fed transfer reaction decay probabilities (Fig. 12). In contrast to ^{241}Pu*, fission decay is now the dominant process above S_n whereas capture decay, representing only one third of the total, drops continuously and even more steeply above the neutron "inelastic" emission threshold energy (the capture cusp is well visible around 8 keV). Regarding the SWFCF pattern as function of excitation energy, one observes in Fig. 13 trends similar to fertiles except in terms of magnitude, in which
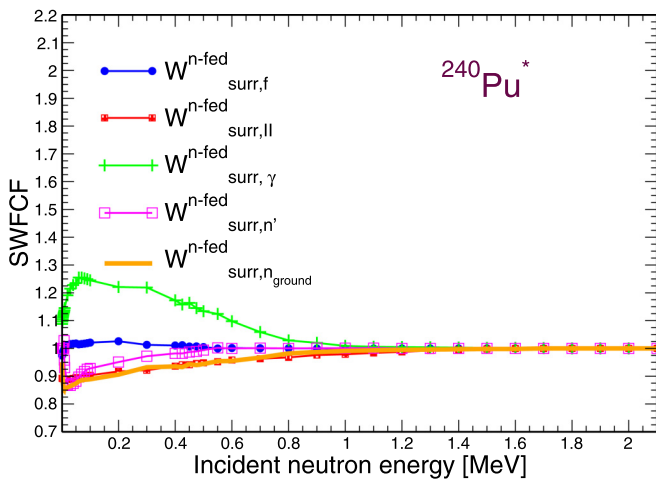
FIG. 13. Comparison of the $W_{\text{surr},f}$, $W_{\text{surr},II}$, $W_{\text{surr},\gamma}$, $W_{\text{surr},n}$ and $W_{\text{surr},n'}$ patterns corresponding to the neutron-fed surrogate-reactions decay probabilities according to the ^{240}Pu*.
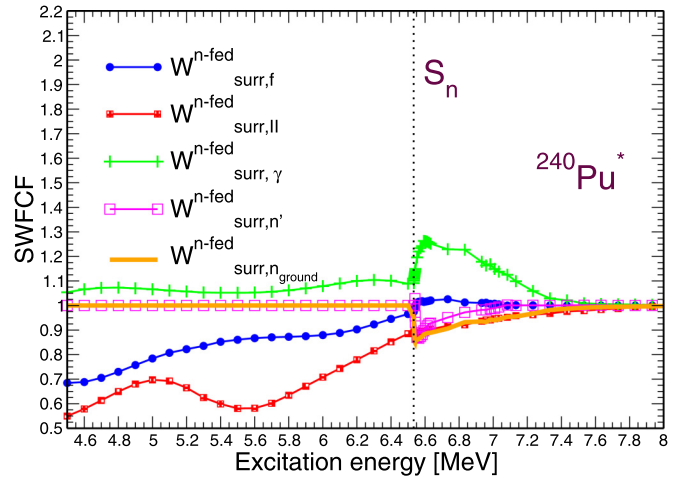
FIG. 14. Same as Fig. 13 but over the whole excitation energy range. One remarks the opposite sign correction between $W_{\text{surr},f}$ and $W_{\text{surr},\gamma}$ and the significant $W_{\text{surr},II}$ correction below S_n.

the variation envelope remains limited [$^{+30}_{-10}$%]. This indeed contrasts with fertile isotopes in which fission barrier heights, lying above neutron emission threshold, reduce strongly the number of open fission channels and thus deliver a larger amount of width fluctuation correction at low neutron energy (cf. Fig. 11).

3. Overview of neutron subthreshold WFCF features

At this stage, it is interesting to recall that our main objective is high-quality simulation of surrogate-reaction probabilities as the SRM does not impose width fluctuations and W_{II} corrections treatment. One realizes that digging under neutron emission threshold requires an extension of Fig. 13 down to low excitation energy. As far as one benchmarks SWFCF results by feeding the calculations with the incident neutron excited state population, one observes for $W_{\text{surr},II}$ limited impact over the range S_n to $(S_n + 1 \text{ MeV})$ but increasing negative correction as the excitation energy decreases (larger than 30% on Fig. 14). Since the flux that can be redistributed from the fission channel to the γ channel shrinks dramatically (Fig. 15), the enhancement of radiative decay remains moderate and constant ($\approx$10%).

As conclusion to this paragraph, I have shed light on SWFCF features as assumed in the WFCF extreme limit [Eq. (13)] that one is not usually accustomed to dealing with. I have shown that both radiative and fission decays can now endorse the role of the enhanced channel with positive enhancement as large as 100% (fertile nuclides) right above S_n.

B. Low excitation energy reaction decay Monte Carlo probabilities

Validity of the SRM hypotheses has been discussed quite extensively in the past decade (see the review by Escher *et al.* [9], the measurements by Kessedjian *et al.* [35], Boutoux *et al.* [18], and Ducasse *et al.* [20], for instance). This section aims to revisit this question with a view of the present robust
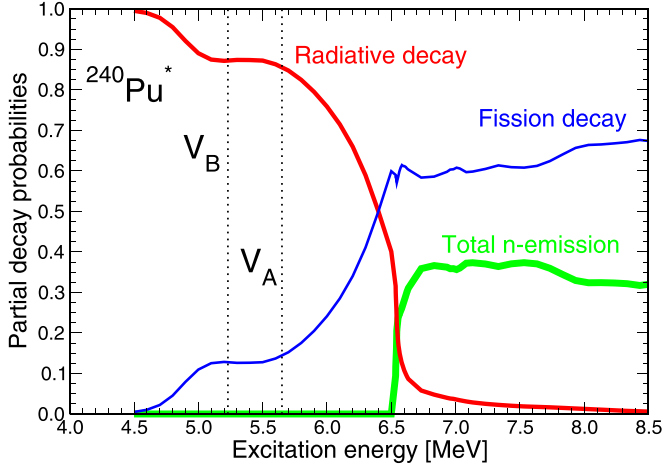
FIG. 15. Same as Fig. 12 but over the whole excitation energy range.

formalism. I now extend this thinking to the joined SWFCF and subthreshold fission effects on calculated transfer reaction probabilities. For this investigation, I keep studying our two examples, namely ^{240}Pu* and ^{241}Pu*, illustrating fissile and fertile categories.

a. Fissile nuclides. The backdrop for fissile nuclides below S_n is simpler since only fission and γ decays compete across Eq. (27). As already specified, in the context of fundamental fission barriers sitting below S_n, fission occurs mainly across discrete Bohr transition states built solely from pure collective excitations (assuming even-even fissioning nucleus) that were carefully generated using the procedure described in Ref. [11]. Collective vibrations are of several kinds, beginning with the *zero-vibration ground state* (of spin-parity projection on the fissioning nucleus elongation axis $K^\pi = 0^+$), then involving low excitation energy collective vibrations such that the γ-*axis vibration* ($K^\pi = 2^+$), the *mass-asymmetry* ($K^\pi = 0^-$), the *bending* ($K^\pi = 1^-$), and even the *octupole* vibration ($K^\pi = 2^-$). All of them, combined or not, supply bandheads for the rotational band structure under classical J^π building rules as noted below:

$$J^\pi = \begin{cases} K^\pi, (K+1)^\pi, (K+2)^\pi, \ldots & \text{for} \quad K \neq 0 \\ 0^+, 2^+, 4^+, \ldots & \text{for} \quad K = 0^+ \\ 1^-, 3^-, 5^-, \ldots & \text{for} \quad K = 0^-. \end{cases} \quad (29)$$

^{240}Pu* is very specific in the way that according to neutron-incident s waves, two J^π states can be excited: 0^+ and 1^+. Low neutron energy fission decay magnitude is then correlated to the accessibility of $J^\pi = 0^+$ and 1^+ transition states. Unfortunately, although few $J^\pi = 0^+$ transition states can contribute, the fission across 1^+ transition states play little role. The 1^+ transition state building requires at least combination of two collective phonons on top of the inner saddle (viz., bending associated with mass asymmetry in which the resulting energy is estimated to be 0.7 MeV above S_n). ^{240}Pu* peculiarity is properly told with Figs. 16 and 17, which display the surrogate-reaction individual J^π fission probabilities for positive-parity spins (respectively, negative parities) that satisfy $\sum_{c=f,\gamma,n,n'} P_c^{J^\pi}(E_x) = 1$. One
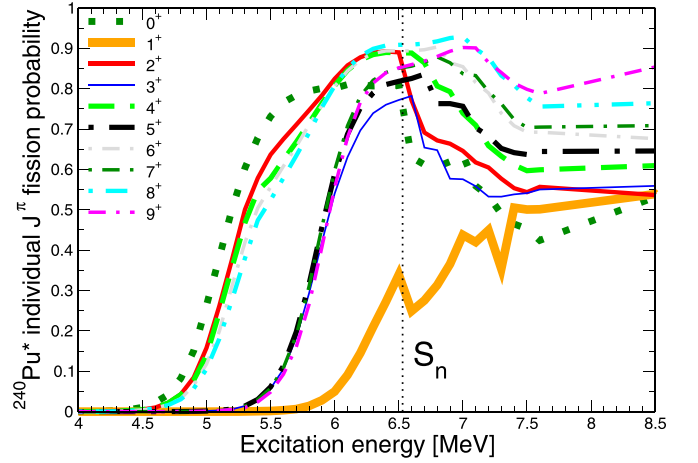

FIG. 16. Monte Carlo $\mathcal{R}$-matrix double-barrier fission surrogate-reaction probabilities of ^{240}Pu* as a function of resonance spin (positive parity) and excitation energy up to neutron kinetic energy of 2.1 MeV. The vertical bar at 6.53 MeV materializes neutron emission threshold. This figure displays in particular the peculiar 1^+ fission barrier probability (orange thick solid curve) that creates an atypical small contribution to the low neutron-incident energy fission cross section. Note: for unbiased illustration, those decay probabilities according to Eq. (27) are fed with an unitary population per J^π.

readily imagines that the decay probability spin-parity independence (WE assumption) cannot be truly satisfied at low excitation energy for this isotope since for positive parities one observes three groups corresponding respectively to total level spin sequences $J = 0, 2, 4, 6, 8$, $J = 3, 5, 7, 9$, and $J = 1$, whereas for negative parities this trend is restrained to two groups with the first group merging all spins except zero spin. The 0^- peculiarity must be granted in the absence of 0^- states in the discrete transition state spectrum of even-even compound nuclei since Eq. (29) prevents construction of any
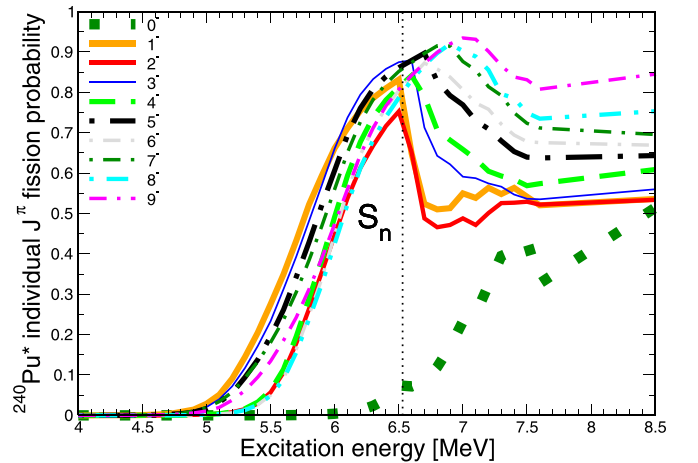

FIG. 17. Same as Fig. 16 but for negative parity. The figure shows the 0^- probability [green-dotted (lowest) curve] which has a singular low excitation energy range contribution solely due to tunneling fission across continuum transition states.
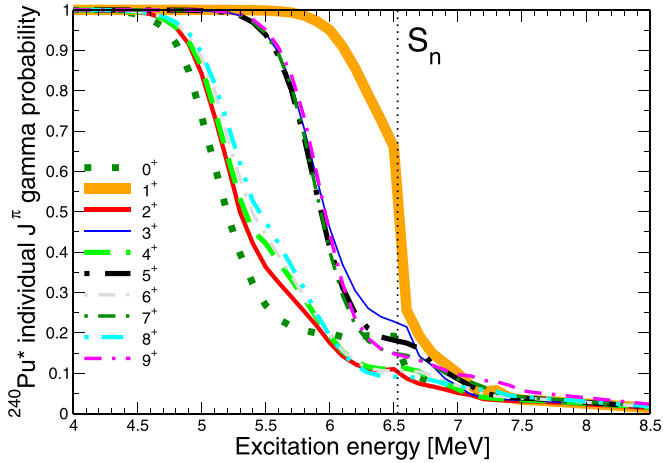
FIG. 18. Monte Carlo $\mathcal{R}$-matrix γ-decay surrogate-reaction probabilities of the $^{240}\text{Pu}^*$ as a function of the resonance spins of positive parity and excitation energy up to the neutron kinetic energy of 2.1 MeV. The vertical bar at 6.53 MeV draws the neutron emission threshold.

of those quantum numbers below the nucleon pair breaking energy.

In terms of γ-decay surrogate-reaction probabilities, total flux conservation imposes below S_n reciprocal response to the fission. This statement can be verified on respective positive (Fig. 18) and negative (Fig. 19) parity excited states γ-decay probability plots where the three and two groups of probability patterns are recovered. Above S_n, cusps in γ- and fission decay probabilities due to neutron emission opening (refer to Figs. 20 and 21) are well visible on corresponding figures. Since the entrance population was chosen unitarily, neutron emission probability magnitude and energy threshold differences are solely due to l relative orbital momentum dependency from one side and the competition between fission and γ decay channels from the other side. The former statement is ruled by Eq. (9) supplemented by our hypothesis on S_l value even-odd dependence. The latter statement explains the larger neutron emission probability
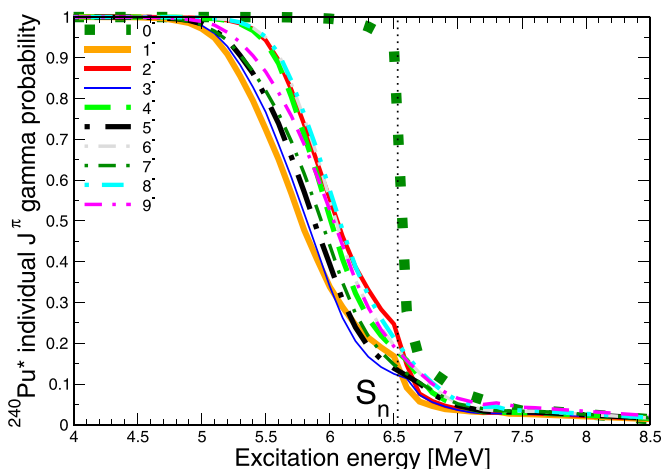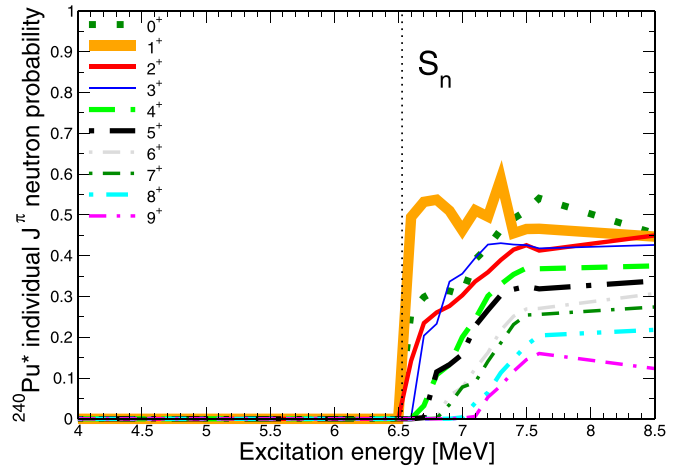

FIG. 20. Same as Fig. 18 but for neutron emission from positive-parity excited states.

magnitudes encountered both for 0^- (Fig. 21) and 1^+ (Fig. 20) since competitive fission channel probabilities at S_n remain much lower than other reaction probabilities. Finally, from the pictures above, it is hard to conclude that the WE limit is ever reached as excitation energy increases since fission and neutron emission decay probabilities keep exhibiting large spreading as far as the associated γ decay probabilities collapse.

b. Fertile nuclides. Odd-neutron isotopes are characterized by low excitation energy combination of single-quasi-neutron states with collective vibrations. One expects fewer transition state fission spectrum oddities because of the dissimilar nature of quasiparticles as well as denser level density right above the Fermi energy. Figure 22 illustrates combinatorial QPVR [11] level densities simulated as a function of nucleus character, which brings more arguments to the debate. As the low-energy spectrum is denser (odd-odd nuclei), it should more quickly tend toward the statistical regime where decay of the nucleus is dominated by statistical level density. Within

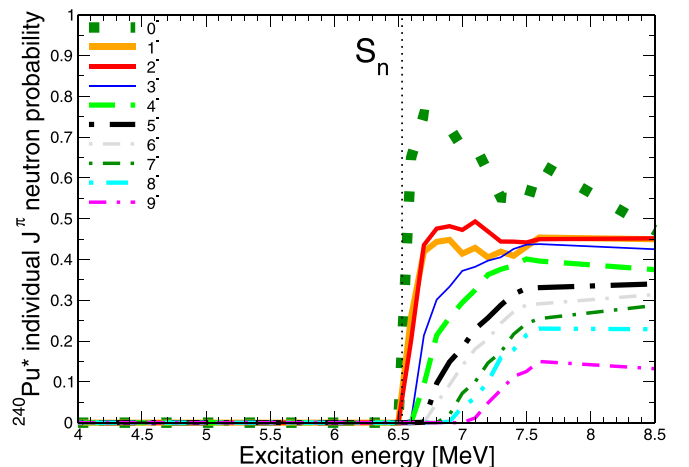FIG. 19. Same as Fig. 18 but for negative-parity excited states.

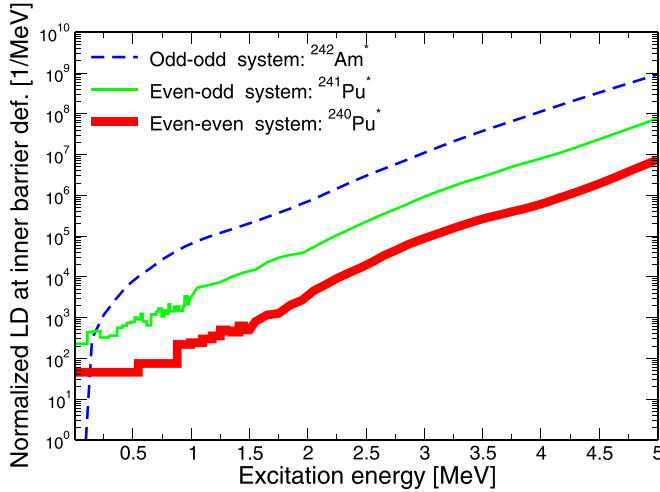FIG. 21. Same as Fig. 18 but for neutron emission from negative-parity excited states.

FIG. 22. Combinatorial quasiparticle-vibrational-rotational level density predictions on top of inner barrier corresponding to even-even (^{240}Pu*, red thick solid curve), even-odd (^{241}Pu*, green thin solid curve), and odd-odd (^{242}Am*, blue dashed curve) nuclei.

such a regime, spin-parity probability dependency is likely of less importance, because tens of fully opened transition states for a given spin parity and fission barrier tunneling strengths balance each other. More than 250 bandheads are counted within the 0- to 1-MeV range on top of the inner barrier, according to an even-odd fissioning nucleus. Relevant fission decay probabilities across positive (Fig. 23) and negative (Fig. 24) parity transition states show two groups of curves associated respectively to discrete and continuum ($J > 6.5\hbar$) energy ranges. For full understanding, we must explore also γ- and neutron-decay probabilities shape patterns.

One remembers that the neutron emission width is related to the reduced width amplitude such that $\Gamma_n^{1/2} \equiv \gamma_n \sqrt{2P_l}$ with
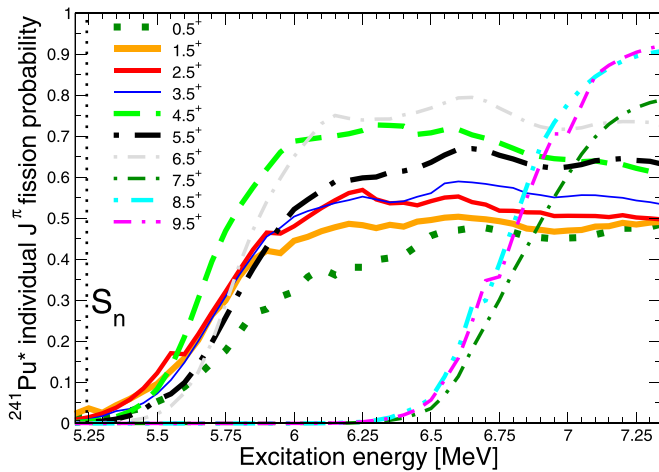

FIG. 23. Monte Carlo $\mathcal{R}$-matrix double-barrier fission surrogate-reaction probabilities of the ^{241}Pu* as a function of resonance spins (of positive parity) and excitation energy up to the neutron kinetic energy of 2.1 MeV. The vertical bar at 5.24 MeV sets the neutron emission threshold.
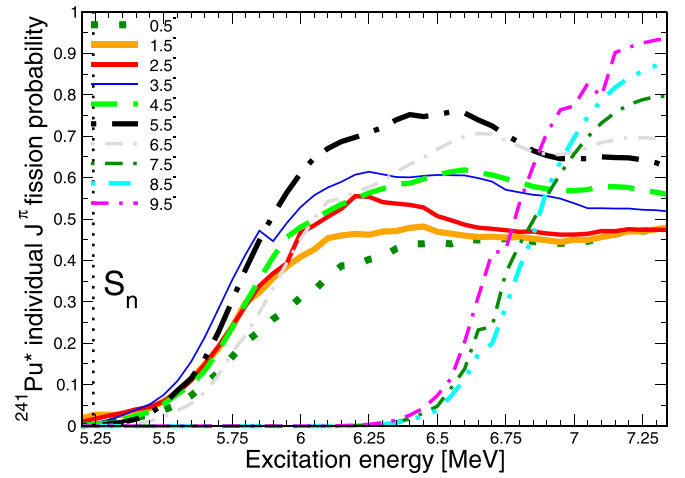

FIG. 24. Same as Fig. 23 but for negative-parity excited states.

P_l, the relative orbital angular momentum-dependent centrifugal penetrability. In compliance with Eq. (10), one addresses $\overrightarrow{J}_{A+1} = \overrightarrow{I}_A + (\overrightarrow{i}_n + \overrightarrow{l}_n)$. Applied to even-even residual nucleus ($I_A = 0$), high J_{A+1} can be reached only when l_n increases. Since the centrifugal barrier penetrability decreases as l_n increases, neutron emission is blocked at low energy for large l_n values. This well-known allegation is verified in Figs. 27 and 28. For high spin value, fission decay is negligible below 6.5 MeV, restricting the question to a γ decay and neutron emission dual competition. In this configuration, the γ-decay probability is then exactly the reciprocal of the neutron emission probability (clearly manifest when comparing Figs. 25 and 27 and Figs. 26 and 28), which acts as the driver of the γ-decay channels. When both neutron emission and fission coexist, fission competes strongly with neutron emission as illustrated by the $J^\pi = 9.5^+$ curves on Figs. 23 and 27. Indeed, neutron emission reaches its maximum when continuum fission opens at 6.5 MeV while the γ drop is still reinforced.
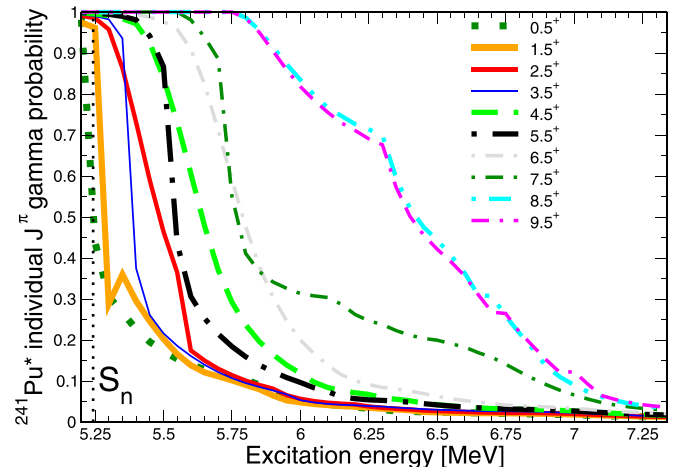

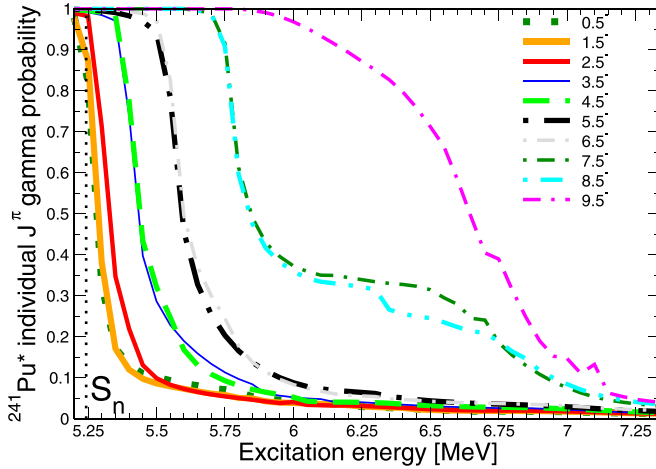FIG. 25. Same as Fig. 23 but for γ decay from positive-parity excited states.

FIG. 26. Same as Fig. 23 but for γ decay from negative-parity excited states.

FIG. 28. Same as Fig. 23 but for neutron emission from negative-parity excited states.

Final γ decay is driven by fission and/or neutron emission; this can be justified by the very low sensitivity of the γ decay width to the initial-state spin parity. Indeed, at high excitation energies (>5 MeV), level density for the nucleus in the ground state is quite large and there is somehow an equiprobability for γ cascade from any spin-parity state so that the γ-decay probability is being adjusted to external constrains. In contrast, at about S_n excitation energy, neutron emission is absolutely ruled by the centrifugal barrier penetrability while fission is driven essentially by barrier tunneling at large nucleus deformation, following the Aage Bohr [16] postulate.

C. Monte Carlo simulation of surrogate-reaction measured probability

I remember from the analytical formulation of the probability [Eq. (25)] that three main ingredients have to be weighted to evaluate the validity of the SRM [Eq. (6)] for neutron-induced cross-section inference. In the sections
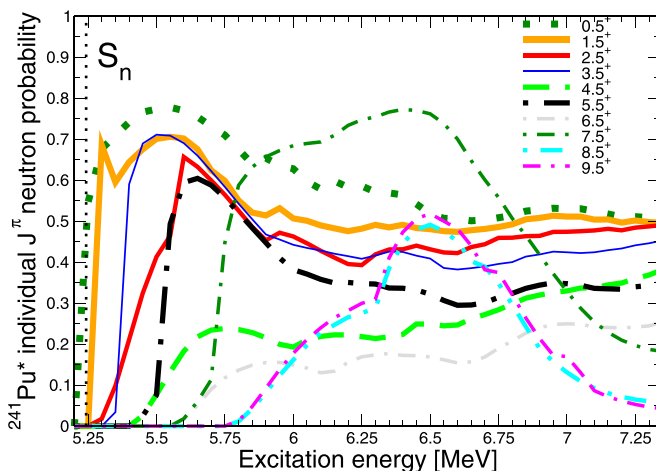

FIG. 27. Same as Fig. 23 but for neutron emission from positive-parity excited states.
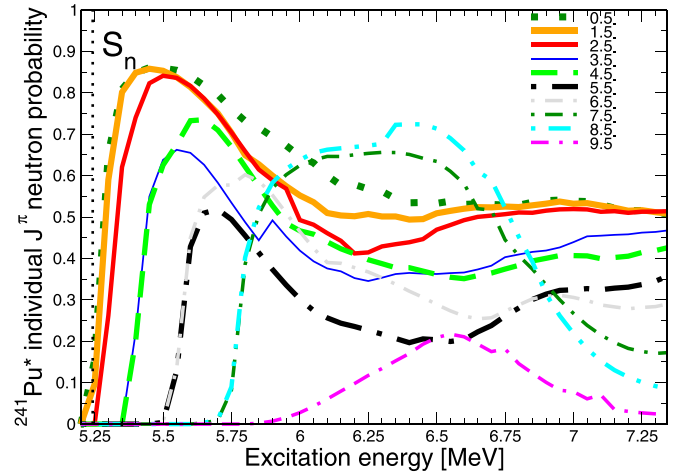
above, two out of three ingredients have been examined, leaving the consequence of nonuniform excited nucleus state population across $\mathcal{F}_{\mathrm{surr}}^{A^*}(E_x, J, \pi)$ to be assessed. I have recalled in Sec. III A that neutron-induced and direct reactions carry their own total angular momentum population distributions. The former J^π distribution profile is sharp and centered about $J_{A+1} \approx I_A$ (Fig. 1) at low neutron energy,[7] whereas a direct reaction population distribution is rather broad and centered about a high total angular momentum value (Fig. 3) since the transferred relative angular momentum is at least of 3 units. From this general trend, I must distinguish the peculiar case of (t, p) reactions on even-even target nuclei that verify rather single parity per J given (Fig. 2). To estimate the bias carried by the sensitive choice of the given population distribution along the neutron cross-section inference on the ground of Eq. (6), I have carried the surrogate-reaction probability simulation all the way following Eq. (27) for the three typical spin-parity population distributions of Fig. 3 according to ^{240}Pu* and a fourth distribution called uniform that is now unitary on the grounds of Eq. (7). I expect the ^{240}Pu* to supply representative and maximum impact of the approximations involved since it covers the excitation energies below S_n, preferentially the excited states reached with low-energy neutrons (close to zero $\hbar$) and also the discrete transition state spectrum that is for this nucleus sparse and built solely from collective degree-of-freedom motions. For best illustration, the results are benchmarked against the neutron-entrance distribution entailed by the SRM. Although feeding neutron-induced population fractions for excitation energies lower than S_n is meaningless, calculations are made according to the distribution at S_n for present demonstration. Figures 29 and 30 are respectively drawn according to fission and γ-decay

---

[7]Low-energy neutron-induced distributions are centered about values of low spin (case of even-even targets) or values of high spin when the intrinsic spin carried by the target is high (example of the ^{235}U neutron target).
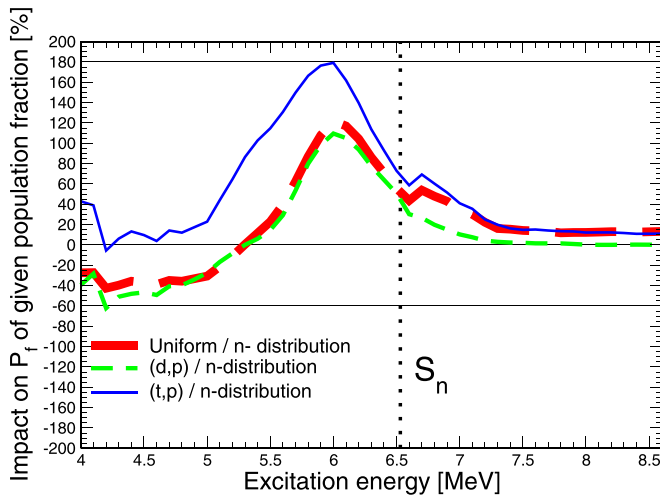
FIG. 29. Biais estimation [%] on calculated fission decay probabilities of the ^{240}Pu* according to the choice of a given population distribution by reference to the neutron-induced population as calculated by the LNG code. The latter regarding excitation energies lower than S_n corresponds to the one at S_n that supports mainly 0^+ and 1^+ excited levels by s waves (24% and 73% respectively of total fraction). The (d, p) and (t, p) distributions information are extracted from Refs. [22] and [3] respectively, whereas the uniform distribution is set on the ground of Eq. (7).

probabilities. One immediately observes that the broadest entrance distribution, (d, p), returns as expected, similar to the uniform distribution. The peculiar (t, p) population distribution is the one that impacts most significantly the fission probability with a deviation from the reference up to 180% below S_n. It happens that using a (n, f) population rather than, for instance, the (d, p) population, generates errors of opposite signs, with maxima of $+120\%$ below S_n in terms of fission and -60% in terms of γ decay. However, above S_n, swapping distributions generates smaller biases than one could have ascribed according to this ingredient ($<40\%$). One
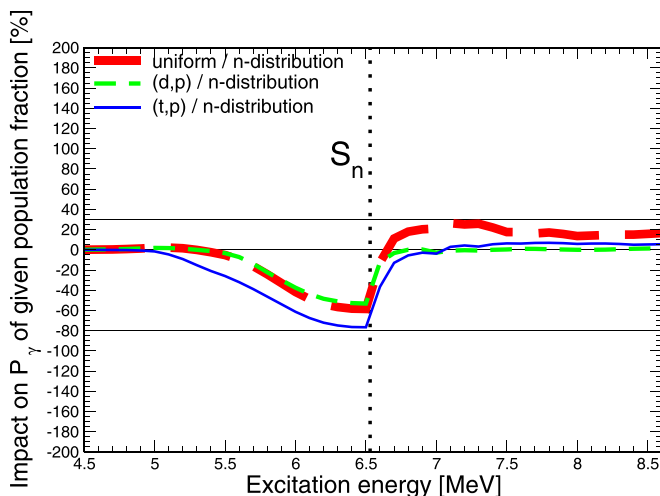

FIG. 30. Same as Fig. 29 but according to the γ-decay reaction.

can notice that the latter bias goes the same way regardless of whatever P_f or P_γ are considered.

V. SUMMARY AND PERSPECTIVES

In this paper, I have emphasized the actual possibility of carrying out one-dimensional fission barrier extended $\mathcal{R}$-matrix Monte Carlo simulations of neutron-induced cross sections jointly with surrogate-reaction decay probabilities. If I omit the question of γ-decay probabilities, which are to be discussed in a future publication, it is manifest that evaluating simultaneously experimental neutron-induced cross sections and fission decay probabilities will definitively help assess nuclear parameters for fissile nuclides which have fission thresholds not accessible by NS techniques and for target material with unsuitable lifetimes or with high radio toxicity. The latter statement has been frequently put forward in literature but also strongly questioned because of the technique used (SRM) in analyzing surrogate-reaction data. The present Monte Carlo approach does not suffer from such a historical approach, which should be weeded out in next-generation evaluations. However, I am aware of the need to pursue efforts on direct reaction modeling, in which reliability remains a genuine challenge.

Beyond the Monte Carlo approach, a simpler comparison with the more conventional analytical formulation of decay probabilities has quantified the main biases brought by the SRM hypotheses as far as heavy isotopes are concerned, namely on the excited nucleus spin-parity state population distribution, on the in- and outgoing channel width fluctuation correction factor, and finally on the shape of individual decay probabilities. In terms of population distribution, replacement of the peculiar (t, p) and (d, p) direct reaction distributions by the neutron-incident distribution generates large biases, especially below S_n for fissile isotopes, on calculated probabilities. Impact of the SWFCF formulation, more appropriate for surrogate-reaction treatment than classic WFCF equations, can be quite significant on the inference process for neutron cross-section prediction. It is worth noting that radiative and fission decays have now endorsed the role of the enhanced channels. Regarding WE, which suggests no spin and parity BR dependency, this statement in terms of fission probability is strongly correlated with the N-Z character of the fissioning nucleus. This statement definitively fails for e-e fissioning nuclei over the discrete transition states energy range. For some peculiar cases such as ^{240}Pu*, one must guard against the belief that SRM inference matches in terms of fission [35] as good as it is poor in terms of capture reaction [18,20]. In conclusion, I can say that validity of the SRM relies on the overall bias brought by the three main ingredients of Eq. (25), which have a definitive impact that cannot be evaluated precisely for heavy isotopes by common decoupling, as acknowledged from the analytical formula. This reinforces the present surrogate-reaction decay simulated probabilities based on efficient Monte Carlo sampling of nuclear structure parameters fed by sound spin-parity excited state population distributions.

The practical application of the present approach to the Pu fissile isotope family over the 4- to 8-MeV excitation energy range is the topic of a companion publication [36]. The

latter includes, in particular, the modeling of the β-vibrational resonances observed in the fission decay probabilities. In this paper, I do not cope with observed γ-decay probabilities because of the historical absence of such experimental data, but new perspectives on that era have opened up recently [20]. Some partial feedback on this question was already unveiled over preliminary analysis [37] of recent experiments [20] collecting simultaneously γ- and fission-decay probabilities according to the ^{238}U(^{3}He, ^{4}He)^{237}U* reaction. Additional work is ongoing on that matter.

[1] J. D. Cramer and H. C. Britt, Nucl. Sci. Eng. **41**, 177 (1970).

[2] H. C. Britt, W. R. Gibbs, J. J. Griffin, and R. H. Stokes, Phys. Rev. **139**, B354 (1965).

[3] B. B. Back, O. Hansen, H. C. Britt, and J. D. Garrett, Phys. Rev. C **9**, 1924 (1974).

[4] H. C. Britt and J. B. Wilhelmy, Nucl. Sci. Eng. **72**, 222 (1979).

[5] V. F. Weisskopf and D. H. Ewing, Phys. Rev. **57**, 472 (1940).

[6] W. Younes and H. C. Britt, Phys. Rev. C **67**, 024610 (2003).

[7] W. Younes and H. C. Britt, Phys. Rev. C **68**, 034610 (2003).

[8] M. Petit, M. Aiche, G. Barreau, S. Boyer, N. Carjan, S. Czajkowski, D. Dassié, C. Grosjean, A. Guiral, B. Haas *et al.*, Nucl. Phys. A **735**, 345 (2004).

[9] J. E. Escher, J. T. Burke, F. S. Dietrich, N. D. Scielzo, I. J. Thompson, and W. Younes, Rev. Mod. Phys. **84**, 353 (2012).

[10] P. Romain, H. Duarte, and B. Morillon, Phys. Rev. C **85**, 044603 (2012).

[11] O. Bouland, J. E. Lynn, and P. Talou, Phys. Rev. C **88**, 054612 (2013).

[12] W. Hauser and H. Feshbach, Phys. Rev. **87**, 366 (1952).

[13] N. Bohr, Nature (London) **137**, 344 (1936).

[14] A. Foderaro, *The Elements of Neutron Interaction Theory* (MIT Press, 2003).

[15] S. Hilaire, C. Lagrange, and A. J. Koning, Ann. Phys. **306**, 209 (2003).

[16] A. Bohr and B. R. Mottelson, Phys. Rev. **90**, 717 (1953).

[17] O. Bouland, J. E. Lynn, and P. Talou, Nucl. Data Sheets **118**, 211 (2014).

[18] G. Boutoux, B. Jurado *et al.*, Phys. Lett. B **712**, 319 (2012).

[19] O. Cabellos, P. Fernandez, D. Rapisarda, and N. Garcia-Herranz, Nucl. Instrum. Methods Phys. Res., Sect. A **618**, 248 (2010).

[20] Q. Ducasse, B. Jurado, M. Aïche, P. Marini, L. Mathieu, A. Görgen, M. Guttormsen, A. C. Larsen, T. Tornyi, J. N. Wilson *et al.*, Phys. Rev. C **94**, 024614 (2016).

[21] P. A. Moldauer, Phys. Rev. **123**, 968 (1961).

[22] B. L. Andersen, B. B. Back, and J. M. Bang, Nucl. Phys. A **147**, 33 (1970).

[23] J. E. Lynn, *The Theory of Neutron Resonance Reactions* (Clarendon Press, Oxford, UK, 1968).

[24] A. K. Kerman and K. W. McVoy, Ann. Phys. **122**, 197 (1979).

[25] L. Dresner, Columbia University Internal Report No. CU-175, New York (1957), p. 71; see also Resonance Absorption of Neutrons in Nuclear Reactors, Oak Ridge National Laboratory Internal Report No. ORNL-2659 (1959).

[26] J. E. Lynn, in *Proceedings of the International Conference on Nuclear Data for Reactors*, Helsinki, USA, 15–19 June 1970 (IAEA, Vienna, 1970), pp. 93–113.

[27] D. L. Hill and J. A. Wheeler, Phys. Rev. **89**, 1102 (1953).

[28] P. Möller, A. J. Sierk, T. Ichikawa, and H. Sagawa, At. Data Nucl. Data Tables **109–110**, 1 (2016).

[29] R. Capote, M. Herman, P. Obložinský, P. G. Young, S. Goriely, T. Belgya, A. V. Ignatyuk, A. J. Koning, S. Hilaire, V. A. Plujko *et al.*, Nucl. Data Sheets **110**, 3107 (2009).

[30] S. Bjørnholm and J. E. Lynn, Rev. Mod. Phys. **52**, 725 (1980).

[31] J. E. Lynn and B. B. Back, J. Phys. A: Math. Nucl. Gen. **7**, 395 (1974).

[32] C. E. Porter and R. G. Thomas, Phys. Rev. **104**, 483 (1956).

[33] A. Gilbert and A. G. W. Cameron, Can. J. Physics **43**, 1446 (1965).

[34] J. E. Lynn, P. Talou, and O. Bouland, Phys. Rev. C **97**, 064601 (2018).

[35] G. Kessedjian, B. Jurado, M. Aiche, G. Barreau, A. Bidaud, S. Czajkowski, D. Dassié, B. Haas, L. Mathieu, L. Audouin *et al.*, Phys. Lett. B **692**, 297 (2010).

[36] O. Bouland (unpublished).

[37] O. Bouland and B. Jurado, EPJ Web Conf. **146**, 04023 (2017).